Electrostatic Discharge Ground Test of a Polar Orbit Satellite Solar Panel

Mengu Cho[1], Jeong-ho Kim[2], and Satoshi Hosoda[3].
Kyushu Institute of Technology, Kitakyushu, 804-8550, Japan

Yukishige Nozaki[4]
NEC-Toshiba Space Systems Ltd., Tokyo, 183-8551, Japan

and

Takeshi Miura[5], Takanori Iwata [6]
Japan Aerospace Exploration Agency, Tsukuba, 305-8505, Japan

Abstract

The Advanced Land Observing Satellite (ALOS) that was launched by the Japan Aerospace Exploration Agency in 2006 carries a large solar array paddle of 22m x 3m in polar orbit. The wake side of the solar paddle can be charged to a negative value exceeding -1000V. Numerical simulations and laboratory experiments are carried out to investigate charging and arcing phenomena on the backside of the solar paddle that has exposed bypass diode boards and Silver-Teflon® thermal film. Possibility of secondary arc and surge voltage between hot and return ends of power circuit has been investigated. We irradiate solar panel coupons with an electron beam to simulate charging situation near the North Pole. Surface flashover is observed once the insulator potential exceeds -7000V. We have also tested charging situation near the South Pole, where Carbon Fiber-Reinforced Plastics (CFRP) surface facing dense ionospheric plasma may arc easily once a satellite potential drops to -80 or -90V. The solar paddle design has been modified to increase the safety margin against arcing and tests have been carried out to identify the strength limit under extremely harsh test environment.

I.   Introduction

Loss of ADEOS-II (Midori-II) due to power failure [1] resulted from spacecraft charging in the aurora zone has made us reinvestigate strength of polar orbiting spacecraft against spacecraft charging. The risk of charging is

---

indeed increasing for recent polar orbiting satellites that demand more power for spacecraft operation. The increased power means increased risk of catastrophic failure in power distribution system that was demonstrated unfortunately by the loss of ADEOS-II. The increased power also means increased size of solar array paddle. The polar orbit is a peculiar orbit where low energy but dense ionospheric plasma and high energy but dilute aurora particles coexist. As a satellite passes by the aurora zone, combination of plasma wake, non-conductive surface, and aurora particles may lead to severe surface charging of the wake side of the solar paddle. Also if the aurora electron current surpasses the current due to ionosphereic ions, the satellite body itself may be charged to a negative potential.

The Japan Aerospace Exploration Agency (JAXA) launched ALOS (Advanced Land Observing Satellite) in January 2006 to a sun-synchronous orbit of 690km altitude with the inclination of 98.2^o and the 10:30 local sun-time of descending node. Aurora charging has been discussed previously for Freja and Defense Meteorological Satellite Program (DMSP) satellites[2], [3]. Severe negative charging of satellite body was observed for those satellites when the satellites crossed the aurora zone between 65 and 75 degrees of the magnetic latitude and ionospheric ion density decreased as low as the order of 10^9m^{-3}. The orbital altitude of ALOS is not as high as Freja or DMSP. Therefore, ion density would not be as low as Freja or DMSP, which makes it unlikely for a satellite at the same altitude of ALOS to suffer charging similar to Freja or DMSP. ALOS, however, will carry a large solar paddle whose size is 22m x 3m, that is one of the largest solar paddles ever flown in Low Earth Orbit (LEO) except International Space Station (ISS). Figure 1 shows an illustration of the satellite.

Many of recent satellite failures are attributed to malfunction of power system. This is partly because the satellite power has recently increased, often exceeding 10kW. Nowadays, satellite power system designers must consider secondary arc phenomena. When severe spacecraft charging occurs, an electrostatic discharge may occur mostly at a junction of exposed metallic parts and insulator surface. One example of such junction is solar cell electrode and coverglass. A pulse of discharge current flows between the spacecraft and surrounding space plasma. The current is concentrated to a small spot on the metallic surface, which resembles vacuum arc. The discharge current is finite because its energy source is electrical charge stored on external insulator surface of spacecraft. If the discharge ends as a pulse current between the spacecraft and the surrounding plasma, we call it "*primary arc*". When a primary arc occurs between two metallic points that are connected to the power circuit and have different potentials, the arc plasma may short-circuit the power circuit. Then the spacecraft power supply, i.e., solar array, provides energy to the arc plasma. If a primary arc leads to short-circuit, we call it "secondary arc". The secondary arc is divided into three stages as illustrated in Fig. 2. The first is "*non-sustained arc*" where the short-circuit

current flows through the arc plasma only while the primary arc current exists. The second is "*temporary sustained arc*" where the short-circuit current flows even after the primary arc current stops, though it does not continue indefinitely. The third is *"permanent sustained arc"* where the short-circuit current keeps flowing until the power supply is terminated. The permanent sustained arc produces low resistance arc tracks and often leads to complete loss of the electrical output from the power circuit.

Near the North and South Poles, the ALOS solar paddle surface is almost perpendicular to the flight direction so that the paddle faces directly to the sun. Plasma wake is formed behind the paddle, where ionospheric ions that flow supersonically relative to the satellite cannot enter easily. On the other hand, aurora electrons can enter the wake relatively freely because of their high energy of the order of keV or higher. If the wake side has non-conductive surface, the surface can be charged to a highly negative potential, which was pointed out previously via a numerical study by Wang et al [4]. Unless the aurora electron flux becomes extremely high, the satellite body is well grounded to the ionospheric plasma. In this case, the satellite body connected to the negative end of solar array circuit has a negative potential of the solar array output voltage [5]. Therefore, at the wake side severe differential charging is possible between non-conductive surface and conductive surface that is connected to the satellite ground. Solar paddle has many parts of non-conductive surface, such as coverglass, insulator sheet underneath solar cells and thermal film. For the case of ALOS orbit as shown in Fig.3, the differential charging is more severe near the North Pole where the solar paddle back surface that receives no sunlight is in the wake side. Near the South Pole, the front surface (i.e., surface with solar cells) is in the wake side. Therefore, photoelectrons relax the negative charging of the non-conductive surface (i.e., solar cell coverglass) compared to the situation in the North Pole, though differential charging still occurs if the aurora electron flux becomes very high.

There are four possible cases of severe surface charging for ALOS. We list each case in Table 1. In the table, the normal potential gradient means that insulator potential is more negative than satellite potential. On the other hand, the inverted potential gradient means that insulator potential is more positive than satellite potential. Also in the table, the test environment indicates a method used to charge insulator to produce each potential gradient condition in our laboratory tests. Near the North Pole, the backside insulator (e.g., thermal film) can have normal potential gradient in the wake side. The plasma density and neutral density are much lower than the ram side. At the same time, the front side insulator (e.g., coverglass) can have inverted potential gradient because the ionospheric ions can easily keep the charging potential of the coverglass nearly equal to the plasma potential while excessive aurora electrons drive the satellite potential to a negative potential. Near the South Pole, the backside

now facing the ram direction can have inverted potential gradient and the front side can have inverted potential gradient.

The ALOS solar paddle consists of nine panels that generate a total of 7kW at End-Of-Life (EOL) condition [6]. Each panel has 8 array circuits. Each array circuit has 159 series cells x2 parallel cells and shares blocking diodes and bypass diodes. There are 72 array circuits for the entire paddle and the total number of cells is approximately 23000. One solar array circuit generates 56 to 58V and 2.7A. (For simplicity, in this paper we approximate the solar array output voltage by 60V.) Solar cells are 69mm x 36mm Si cells that have no integrated bypass function. The bypass diodes are inserted at every 27 cells. The power control unit regulates the power at 55V in the dayside. Between solar cell strings, there is Room Temperature Vulcanizing (RTV) silicon grouting to prevent intra-string or inter-string secondary arc. The solar paddle is made of 25mm thick CFRP/Aluminum honeycomb substrate. The backside has Silver-Teflon® (Ag-TF for the rest of the present paper) thermal control film on the CFRP/Aluminum substrate to alleviate the effect of the Earth's albedo. In addition, there are bypass diode boards at the backside. When the ADEOS-II failure occurred, the ALOS solar paddle was already assembled in a factory. We call this stage of panel design the baseline design in this paper. Coupons were made using the same process and material as the flight solar paddle based on the baseline design. A photograph of a solar array test coupon representative of ALOS solar panel is shown in Fig.4. The bypass diode board and nearby thermal film is shown at the center. This coupon is used in the laboratory experiment that will be discussed later in detail. Electrical wires, Raychem Spec55/AWG(American Wire Gauge)24, run all over the paddle back surface. The wires are attached to CFRP via Silicon adhesive through holes in Ag-TF film.

Reexamination of the baseline design raised several surface charging issues that required simulations and laboratory tests [6]. The backside of the baseline design panel has several potential problems. It is mostly covered with 200mm x 100mm Ag-TF thermal control films and is partially covered with 8 bypass diode boards and wire harness cables transmitting power and signals. Figure 4 shows a test coupon used in the Electrostatic Discharge (ESD) tests. The patches of Ag-TF have the thickness of 51μm and are separated from one another in 2mm spacing. About 3000 films are used for the entire paddle. Since the Ag-TF film used for the ALOS paddle does not have conductive film for its exposed side and its silver-coated side is attached to the CFRP substrate by RTV insulator adhesive, the Ag-TF films pose charging problems of insulator surfaces with significant areas and floating conductors with exposed silver edges as shown in Fig.4. Each bypass diode board has 6 diodes on a glass-polyimide substrate and a pattern of heat sink below the diodes. Silicon white paint mostly covers the surface of the diode board. The diode terminals made of copper, which are exposed to space, are connected to the

ends of the array strings and create the potential differences of up to 60V directly connected to power line on the board. The conductive heat sink is not grounded. As for the bypass diode board, the diode terminals and the heat sink form a potential arcing risk. Secondary arc may occur between the exposed conductive parts of diodes in a similar way to secondary arc between solar array strings [9]. The six diodes are arranged in a zigzag shape of 2 x 3 and the maximum potential difference between two diodes facing each other is 40V.

The major purposes of the ESD tests on the baseline design are to verify that permanent sustained arc would not occur between diode terminals and the surge voltage between power harness lines caused by a primary arc is within an acceptable limit. The surge voltage emerged as a concern because we can no longer ignore inductance and resistance associated with solar paddle power harness considering the paddle length, 22m. The injection of a fast current pulse into power circuit gives rise to a large voltage pulse in the harness line. The surge voltage might exceed the voltage limit across various power electronics devices, such as transistor, diode and others.

We carried out ESD tests for both sides of the ALOS solar paddle shown in Fig.4. In the present report, however, we report only the result of ESD tests carried out for the back side. The front side has a design very similar to ETS8 solar paddle except the amount of additional RTV Silicon adhesive used to encapsulate solar cell edges. Although we also carried out ESD tests for the front side, the results are more or less similar to the ESD tests for ETS8 that was described in detail in [7] and [8] for both the test environments, plasma and electron beam.

In the second section of this paper, we describe the experimental facilities used for the ESD tests. From the third to sixth sections, we describe our investigation of a situation over the North Pole that was simulated by an electron beam in a vacuum chamber to produce the normal potential gradient on the backside of test coupons. The third section describes the experimental results to identify threshold of primary arc inception under the normal potential gradient. In the fourth section we describe numerical simulation carried out to identify the aurora environment that produces the charging level exceeding the primary arc inception threshold. In the fifth section we estimate the number of primary arcs expected in orbit. In the sixth section we describe the experimental results on the secondary arc and the surge voltage. The seventh section deals with a situation over the South Pole that was simulated by low-temperature plasma to produce the inverted potential gradient. In the eighth section, we present experimental results for modified design and describe how we determined the final flight design. In the ninth section, we give overall evaluation of the back-side of the baseline design paddle in terms of insulation strength against aurora charging.

II. Experimental System

For the ESD tests, we used a vacuum chamber of 0.6m diameter and 0.9m length shown in Fig.5. The coupon panel was placed horizontally over an acrylic plate with spacers of 20mm height. Experiments are carried out at room temperature, $20^{o}C$, approximately. The chamber is equipped with an electron gun that can generate an electron beam with energy as high as 30keV. The gun is vertically mounted at the center top of the chamber. Typical beam current density at the coupon surface is $10mA/m^2$ at maximum with 90mm half width. The electron gun is equipped with a shutter system. We can open or close a shutter by sending a pulse signal. The chamber is also equipped with a DC glow discharge plasma source that generates Ar plasma with a density of $2x10^{11}m^{-3}$~$1x10^{12}m^{-3}$ and a temperature of 1eV near the coupon. The chamber is equipped with a turbo molecular pump and a rotary pump. Typical chamber pressure is from $2x10^{-4}Pa$ ~ $2x10^{-3}Pa$ while we use the electron gun and $3x10^{-2}$ Pa ~ $4x10^{-2}Pa$ while we use the plasma source.

In Fig.5, we can see a Trek® surface probe mounted on a PC-controlled x-y stage that can scan the area of 90mm x 70mm at every 10mm interval in one minute. Also in the figure, we can see a spherical Langmuir probe (LP) of 30mm diameter. The direct distance to the coupon surface from LP is 120mm. The LP was used to give an extra energy to arc plasma during the normal gradient experiment with the electron beam and to measure the Ar plasma properties during the inverted potential gradient experiment with the plasma source. The distance of 120mm was rather dictated by the need to measure the plasma properties so that no interference would occur between the sheath from the probe and the coupon. The distance should have been shorter to give the energy more efficiently to the arc plasma but we fixed at one point to give the dual purposes to one probe while keeping consistency among the test results. During the tests, we recorded video image of the coupon surface to a PC using an infrared camera. We can identify all the primary arc locations using self-developed video analysis software on the PC. Current and voltage waveforms were recorded to another PC by a high-speed data acquisition board that can store all the waveform data as long as the arc frequency is less than 30 arcs/s, which usually applied to the present cases. Before and after the coupons were placed in the chamber, the coupon surface was scanned by an optical microscope with 60x magnification. Photographs of entire surface were recorded to a PC with their coordinate.

Table 2 lists combination of circuit diagrams and purpose of each test case. In Figs.6, 7, 8 and 9, we show circuit diagrams labeled in Table 2. The Shunt-OFF circuits (Figs.6 and 8) correspond to solar array circuit that is closest to the satellite body. The purpose of shunt-off configuration is to test secondary arc. The circuit simulates the innermost solar array circuit that is closest to the satellite body. Therefore, inductance, resistance and

capacitance associated with power line of solar array are smallest. The Shunt-ON circuit corresponds to solar array circuit at the far end of the solar paddle. The purpose is to test surge voltage between hot and return lines of the array circuit and power electronics devices such as a shunt transistor. The circuit simulates the outermost solar array circuit that is the most distant from the satellite body. The inductance, resistance and capacitance associated with power and ground lines are the largest. The additional inductance, resistance and capacitance correspond to 22m harness lines. For each solar array string, there are two pairs of hot and return lines. Therefore, we used a pair of 11m parallel lines made of AWG 22 wire (R_{PH}, L_{PH}, R_{PR}, L_{PR} and C_4 in the figures). The resistance, inductance and capacitance labeled R_{IH}, L_{IH}, R_{RH}, L_{RH} and C_5 correspond to harness lines between the paddle drive motor and the shunting device. We used a pair of 0.8m parallel lines made of AWG 22 wire. The resistance, R_{PG}, and the inductance, L_{PG}, correspond to resistance and self-inductance associated with the paddle grounding wire harness. From the measurement of the flight solar paddle, those values are $R_{PG}=0.74\Omega$ and $L_{PG}=10.7\mu H$. We modeled these resistance and inductance by 11m AWG 22 wire. The resistance of AWG 22 wire is 50mΩ/m. Threshold measurement of case 1 was carried out by switching off all the power supplies connected to the external circuit to avoid the risk of discharge between the Trek® probe head and one of the diodes. The shunt switch used in the test circuits are made from electronic parts equivalent, but not identical, to the flight model. They are composed of a NPN transistor, a Zener diode, an inductance and a resistance. The transistor, Tr, is turned on and off by current regulated by another NPN transistor driven by a DC power supply.

The power supply V_1 and V_2 are E4351B solar array simulators that simulate the solar cells connected by the bypass diodes. Strictly speaking, we should connect a solar array simulator to each bypass diode. The main purpose is, however, to investigate the possibility of secondary arc between diodes that has the highest potential difference (40V). Therefore, for simplicity, we used only two solar array simulators. The voltages of power supply V_1 and V_2 are set to 20V and 40V, respectively. The power supply V_3 simulates other solar array circuits and operates at 53V with the maximum current of 2.7A. The resistance R_{DL} simulates the satellite load and the capacitance C_{BC} (=18000μF) simulates the bus capacitance. The value of R_{DL} was adjusted so that the voltages at V_{p1} and V_{p2} are 20V and 40V respectively while a current of 2.7A flows R_{DL} in the shunt-off configuration. Once secondary arc occurs for significant duration, the voltage between the hot and return lines collapses. Then, the diode D_4 is turned on to keep the voltage across the load resistance constant. On the other hand, the diode D_3 works to prevent the current supplied by the power sources V_1 and V_2 from flowing to the load resistance. The diodes D_1 and D_2 are used to protect the power supply. The capacitance C_1, C_2 and C_3 simulate the capacitance

between solar cells in one string and capacitance between cells and substrate. The values are $C_1=C_3=80nF$ and $C_2=800nF$, respectively. The roles of the diodes and the capacitances are discussed in [10].

When an arc occurs, the energy is supplied by electrostatic energy accumulated on insulator surface such as Ag-TF or white paint over the diode board. The coupon size was too small to account for all the insulator surface of solar paddle that could contribute to an arc. The total capacitance of Ag-TF films on the paddle back side is 11μF approximately. In cases 2 and 3, we put the spherical probe as shown in Fig.5. The probe was connected to a high voltage power supply, $V_b(=-7000V)$, and a capacitance, $C_{ext}(=160nF)$. The resistance $R_b(=10M\Omega)$ was to protect the power supply. Once an arc occurred and developed as surface flashover, the arc plasma sometimes reached the probe producing conductive path between the coupon surface and the probe. Then, the energy stored in the external circuit, C_{ext}, was discharged to the arc plasma. The value of C_{ext} was determined to give total energy of 4J, which was determined by assuming one-third of the panel would be charged [4] to threshold value of primary arc inception, -1500V. The inductance and resistance connected to the capacitance was to limit and slow down the current from the probe by considering the fact that the energy is released by surface flashover that propagates with a finite velocity. We used $R_{ext}=4\Omega$ and $L_{ext}=270\mu H$ based on previous works [11].

In cases 4, 5 and 6, the external capacitance was attached to the return line, which is a usual practice for solar array ESD tests investigating an inverted potential gradient situation. The values of R_{ext} and L_{ext} attached to C_{ext} were also $R_{ext}=4\Omega$ and $L_{ext}=270\mu H$. In cases 5 and 6 we biased the coupon panel to $V_b(=-300V)$ with $R_b(=100k\Omega)$. The external capacitance C_{ext} for cases 5 and 6 is 5μF that gives 0.2J of energy. This was determined from the total capacitance of satellite external surface including solar paddle, 70μF, and the threshold of primary arc inception, -80V.

In the experiment under electron beam environment, the current measured at C_{p7}, which was the total current inside the external circuit, triggered oscilloscopes. In the experiment under plasma environment, the rise of coupon potential measured by V_{p5} triggered oscilloscopes. The current probes, C_{p1}, C_{p2}, C_{p3} and C_{p4} can measure current from DC to 10MHz. The current probes, C_{p5}, C_{p6} and C_{p7} can measure between 1kHz and 120MHz. The voltage probes, V_{p1}, V_{p2} and V_{p3} are 50x differential probes. The voltage probes, V_{p4}, was a Trek® surface potential probe that monitored the floating heat sink potential. A cable connected to the heat sink was extracted outside the vacuum chamber through a high voltage feed-through and connected to a copper plate. The Trek® probe measured the potential of the copper plate outside the vacuum chamber. The voltage probes, V_{p5}, was a 2000x high voltage probe. The voltage probes, V_{p6} and V_{p7}, were 1000x and 100x high voltage probes.

III. Primary Arc Threshold under Normal Potential Gradient

Figure 10 shows position of primary arc that occurred during threshold measurement. The peak current was 25mA and the pulse width was 2μs. In this case, the electron beam energy was 3keV. After irradiating the coupon for 10 minutes the insulator surface was scanned with the Trek$^®$ probe. The surface potential marked in Fig.10 was charged to –1500V. For other electron beam energies the insulator surface was mostly charged to a negative value of the electron beam energy –1500V. When the beam energy was low, arcs appear as single flashes originated from individual points. A typical peak value of the arc current measured at C_{p7} in Fig.6 was less than 0.1A with duration of a few μs. Arcs occur mostly along the edge of Ag-TF insulator. As the beam energy is increased to 9keV, we observe surface flashover that covers extensive area of coupon surface as shown in Fig.11. The surface flashover accompanies much brighter flashes than those arcs at low electron beam energy of 3keV and often ends at the edge of Ag-TF or electrical wires on the surface. From these measurements, we have concluded that arc threshold is –1500V for a small arc and –7000V for surface flashover.

Figure 12 shows arc positions observed for one coupon. More than 2000 arcs were recorded for this coupon with the beam energy of 8keV. The most negative insulator surface potential is approximately –7000V. Arcs occurred at the edge of Ag-TF insulator, diode board and electrical wire, where insulator forms triple junction with nearby conductor. In Figs.13 and 14, we show arc spots observed at edge of Ag-TF and the diode board. Because silver layer of Ag-TF is not grounded, once Teflon surface is charged to a negative value, the silver layer also has a negative value almost half the potential of Teflon surface. The side edge of Ag-TF is occasionally shielded by RTV adhesive that displace from the bottom of Ag-TF. But, unless we intentionally shield the side by RTV adhesive, the side edge has exposed silver layer. The silver layer is adjacent to CFRP that is grounded and distance is only 100μm or so. Therefore, once Silver layer acquires a negative potential close to –1000V, a small arc occurs between the silver layer and CFRP. If the charging potential is large, the small arc may evolve to surface flashover that absorbs charge of one or more patches of Ag-TF.

IV. Numerical Simulation

After the launch in early 2006, ALOS is in a sun-synchronous orbit at 690km altitude. The worst charging condition can be identified based on the satellite trajectory. It is known that charging due to aurora particles mainly occur between 60 and 75 degrees of the magnetic latitude. The longer the satellite stays in the aurora zone, the more negatively it is charged. In addition, if the satellite enters the dayside just after the exit from the aurora

zone, the combination of the most negative potential and the beginning of power generation makes the situation the worst case. Therefore, we looked for the case when the satellite stays the longest time in the aurora zone in the night side and enter the dayside just after the exit from the aurora zone.

Figure15 shows an example of satellite trajectory that meets the above-mentioned conditions. This trajectory occurs on January 30th, 2006. At 6:10UT denoted by the closed circle in Fig.15, the satellite exits the aurora zone and enters the dayside at the same time. ALOS stays 1200s inside the aurora zone. As we look at 46 days from December 23rd, 2005, there are five such paths over the North Pole where it stays 1200s before it enters the dayside. The example shown in Fig.15 has the highest geographical latitude when the satellite enters the dayside, 68° latitude and 86° longitude, which probably leads to the most severe charging because the plasma density is the lowest. The year 2006 is also near the bottom of 11-year period solar activity, giving the lowest plasma density at the altitude of 690km. Once we know the satellite position where the worst charging condition is expected, we can obtain the plasma conditions from known models of ionosphere. In Table 3, we list the plasma conditions at 68° latitude and 86° longitude at 6:10 UT on January 30th, 2006 that are taken from International Reference Ionosphere [12]. We use the plasma conditions listed in Table 3 as the reference values for the numerical simulation.

In the numerical simulation, we calculate the charging potential of Ag-TF thermal film at the solar paddle back surface. We use a Particle-in-Cell (PIC) scheme to calculate structure of plasma sheath surrounding the paddle and a particle tracking scheme to calculate current density to dielectric part of the paddle. The basics of the simulation method are the same as Ref.[13]. Because the solar paddle is very long in one direction (3m x 22m), we assume uniformity along the direction parallel to the paddle and consider in a two-dimensional plane that crosses the paddle. Figure 16 illustrates the computational domain. The cross section of solar paddle is given as a rectangular of 3.08m x 0.04m. The domain size is either 20.48m x 10.24m or 20.48m x 20.48m. In both cases, the paddle is placed at the center in y direction and 7 m from the left boundary in x direction. The paddle location and the size of the computational domain were chosen so that the sheath would not overlap with the boundaries and enough space was provided to the wake structure while complying with requirement of computational memory. At the back- and top-sides, there are dielectric surfaces. The dielectric surface at the backside corresponds to Ag-TF thermal film. The dielectric at the topside corresponds to Kapton® tape that insulates the side of aluminum honeycomb substrate. Both the dielectric parts have capacitance of $1.7 \times 10^{-7} F/m^2$ per unit area. The front side has solar cells. We assume sheath from exposed conductor such as an interconnector overlaps and forms one large sheath of –60V that is the solar array generation voltage. The bottom side has deployment synchronization wire

that is grounded to the satellite body. Therefore, the bottom side is also assumed to be –60V. At the backside, there is a small part of conductor that corresponds to CFRP substrate exposed near the paddle edge. Because the substrate is grounded to the satellite body, the exposed CFRP has –60V. At all the four boundaries potential is zero and we assume uniform density ($2x10^{10}m^{-3}$) Maxwellian plasma with a drift velocity of 7.2km/s and temperature of 0.2eV. The computational domain is divided into rectangular meshes of 0.02m x 0.02m.

In the simulation, we calculated temporal evolution of the insulator potential in the following manner:

1. Initial plasma conditions are calculated assuming that all the paddle surfaces have –60V. This corresponds to the situation when the satellite has –60V potential before it enters an aurora zone.

2. Ion current density to each dielectric part is calculated by tracking trajectories of ions from the boundaries. From each grid at the boundary, we inject 1000 test ions. During the particle tracking, electric field distribution inside the domain is fixed assuming that the variation of the field distribution takes much longer time scale than travel time of ions inside the domain.

3. Charge accumulated by aurora electrons at each dielectric part is calculated. We assume, for simplicity, that the current density to each dielectric part is uniform and constant regardless of its position.

4. Surface potential of each dielectric part is calculated from its capacitance and accumulated charge.

5. Field distribution surrounding the paddle is updated using the renewed dielectric potential. The PIC scheme is used to include effects of space charge due to ionospheric plasma. The PIC scheme is run for one ion plasma oscillation period so that the plasma around the paddle adjusts itself to the renewed dielectric potential.

6. The steps 2,3,4 and 5 are repeated until predetermined time expires.

In the above steps, the time steps to update the dielectric surface potential, denoted as dt_L, is taken from 0.1 to 20s depending on the aurora current density that determines the time constant of charging. Table 4 lists the parameters of each simulation. We consider $3.2x10^{-8}A/m^2$ as the nominal value of aurora current density based on analysis of DMSP observation data [14]. The aurora current density, however, has a wide range of variation. The maximum current density can be 5000 times the nominal value, i.e., $1.6x10^{-4}A/m^2$ [14]. We define the aurora flux coefficient a by the ratio of a given aurora current density to the nominal electron current density, $3.2x10^{-8}A/m^2$.

$$a = \frac{j_a}{3.2 \times 10^{-8}} \qquad (1)$$

where j_a is the aurora electron current density in A/m^2.

The energy distribution of aurora electrons is also highly variable. It is very difficult to define a typical energy distribution of aurora electrons. Therefore, we simply assume that the aurora electrons have infinite energy so that they can reach the dielectric surface regardless its potential. This assumption is valid as long as the charging potential is relatively small, of the order of thousand volts.

Figure 17 shows the electric potential distribution around the solar paddle at 880s for case 1 where the aurora current density is the nominal value. The potential of the paddle back surface is zero everywhere, assuring that if the aurora current density remains this low value we can safely ignore the wake charging. The aurora current density is about one-thousandth of the ion ram current density. For such a small amount of electron current, slight amount of ions deflected by the sheath at the side edge of the paddle is enough to cancel the negative charge on the back surface insulator. Therefore, for the nominal conditions of ALOS, arcing on the paddle back-surface in the aurora zone over the North Pole will not occur.

Figure 18 shows the result of case 6 where the aurora current density is assumed the worst. The figure shows the distributions of electric potential and ion density at 9s. The potential of the paddle back surface exceeds -7000V, threshold of surface flashover. Ions form arch-shaped distribution around the paddle as they are attracted from the front side to the back side and rotate along the circular potential structure to conserve their angular momentum. The ions that enter the sheath from the top side of the paddle go to the bottom-side and vice versa. Figure 19 shows temporal variation of the distributions of potential and ion current density along the paddle back surface. Near the top and bottom of the paddle the ion current exceeds the aurora current and locally slows down the charging processes. The ion current at the center, however, is far from canceling the aurora current. Therefore, the paddle back surface potential reaches the surface flashover threshold within 10s for the worst case.

By varying the aurora current density, we looked for the cases where the potential of the paddle back surface reaches –7000V, threshold of surface flashover inception, within 1200s. Figure 20 shows how the paddle back surface potential varies in time for different values of the aurora current density. The bottom and top of the figure correspond to the bottom and top of the paddle back surface, respectively. Initially, the center part attracts ions more than the aurora electrons and reaches zero potential quickly. The bottom and top parts become negative. As time goes on, the negative part moves toward center, because the positions where the incoming ions focus shift in time as the sheath structure near the paddle edges changes. For cases 2 ($a=10$), the maximum negative potential keeps increasing, though it reaches only -600V at 1200s, therefore, no arcing would occur. For case 3 ($a=50$), the back potential exceeds –1000V. The charging does not develop infinitely for this case, because sufficient number of ions is attracted eventually to balance the current against the aurora electrons. As far as the aurora current is

small, the back side potential repeats periodic variation as shown in Fig.20. We observed the periodic variation up to case 4 (*a=200*).

For case 5 (*a=500*), however, the periodic variation does not appear. The maximum negative potential keeps increasing as shown in Fig.20. In this case, the maximum potential reaches -7000V at 160s. Therefore, we conclude that the threshold aurora current density to cause surface flashover is $1.6 \times 10^{-5} A/m^2$, 500 times the nominal value.

V. Number of arcs expected in orbit

We now estimate the number of arcs expected in orbit based on the results of numerical simulation. The Teflon surface potential at time *t* after ALOS enters the aurora zone near the North Pole is given by

$$\frac{d\phi_{TF}}{dt} = \frac{1}{C_{TF}}\left(j_i - j_a\right) - \frac{\sigma_{TF}}{\varepsilon_{TF}}\phi_{TF} \qquad (2)$$

where j_i is the ion current density deflected to the wake region, C_{TF} is the capacitance per unit area, ε_{TF} is dielectric coefficient and σ_{TF} is bulk conductivity of Ag-TF thermal insulator including the adhesive layer between Ag and CFRP. Assuming $C_{TF} = 1.8 \times 10^{-7} F/m^2$, $\varepsilon_{TF} = 2 \times 8.85 \times 10^{-12} F/m$ and $\sigma_{TF} = 1 \times 10^{-16} 1/\Omega/m$, we have

$$\frac{d\phi_{TF}}{dt} \approx -0.18a - 5.6 \times 10^{-6}\phi_{TF} \qquad (3)$$

where we neglected the ion current density compared to the aurora current density. We can also neglect the contribution of conduction current because the conductivity of Teflon is very small. When the aurora current density is so large that the Teflon surface potential reaches the surface flashover threshold, the Teflon surface potential becomes negative monotonically as given by

$$\phi_{TF}(t) = -0.18at \qquad (4)$$

for the cases such as *a>500*. The time to reach the flashover threshold value is given by

$$\tau_{arc} = \frac{7000}{0.18a} \tag{5}$$

Those cases of aurora flux with $a>500$ occur in reality, a few times a year based on data analysis of DMSP SSJ/4 observation [14]. We have estimated a probability density function of the aurora flux value. Table 5 lists the frequency that a satellite encounters the aurora flux higher than each listed value. We define the probability, $F(a)$, that the aurora flux coefficient is less than a by the following equation:

$$F(a) = \int_1^a p(a')da' \tag{6}$$

The probability density function $p(a)da$ denotes probability that the flux coefficient is between a and $a+da$. The function $p(a)$ is given by differentiating $F(a)$ by a. Using the values listed in Table 3, we plot $F(a)$ and its approximation in Fig. 21. By differentiating the approximation formula for $F(a)$, we can approximate the probability density function by the following equation:

$$p(a) = 1.04 \frac{1}{a} \exp(-1.04 \ln a) \tag{7}$$

The number of expected surface flashover in five years is given by

$$N_{arc} = \int_{500}^{\infty} p(a) \frac{T_{path}}{\tau_{arc}} N_{path} da = \int_{500}^{\infty} p(a) \frac{1200 \times 0.18a}{7000} 27000 da = 830 \int_{500}^{\infty} ap(a) da = 1800 \tag{8}$$

where T_{path} is the time spent in each path in the aurora zone near the North Pole, which is assumed to be 1200s and N_{path} is the number of satellite paths that cross the aurora zone, which is assumed to be 27000 (=15path per day and 5years). In Eq.8, the integration was carried out up to 10,000. Because ALOS does not spend 1200s in every path inside the aurora zone, the number given here is the worst possible number. Given the method to obtain the probability distribution function, $p(a)$, the number estimated here contains a wide range of uncertainty. The

number, however, is necessary to carry out the ESD test to check strength of the given solar paddle design against repeated arcs. Assuming T_{path} as 1200s for every orbit would give sufficient margin to cover the upper bound of the uncertainty. This number is used as a reference value when we carry out the tests regarding secondary arc and surge voltage.

VI. Experiment on secondary arc and surge voltage

Figure 22 shows waveform observed when the surface flashover absorbed charge stored in the external circuit. The external capacitance provided current as much as 300A into the solar array circuit for 15μs. The arc plasma momentarily short-circuited the power supply V_2. The current from the power supplies V_1 and V_2, that was measured by C_{p3}, decreased and the currents to the diodes that were measured by C_{p1} and C_{p2} increased, though the currents at C_{p1} and C_{p2} were not fully equivalent to the current, 2.7A, supplied by the power supplies V_1 and V_2. Although the voltage of the solar array simulators measured by V_{p1} and V_{p2} were relatively normal, the current waveforms suggest a temporary sustained arc occurred between diodes. Although we had nearly 1000 arcs with the Shunt-OFF configuration, we had no permanent sustained arc. Only temporary (less than 10μs) sustained arcs similar to the ones shown here were observed.

When a large arc that absorbed charge stored in the external circuit occurred near CFRP substrate under the shunt-on condition, the voltage drop across the ground resistance produced substantial surge voltage inside the array string circuit. The array string circuit and the paddle ground were coupled through capacitance of adhesive and polyimide sheet below solar cells. Nine solar panels of ALOS are grounded to the satellite body via ground wires that has equivalent resistance and inductance of 0.74Ω and 10.7μH, respectively. Figure 23 shows the waveforms measured in various points in the circuit. The charge stored in the external capacitance, C_{ext}(=160nF), was discharged in less than 10μs. A part of the charge was discharged directly to the chamber wall and the rest was discharged through the power circuit to the ground. The current measured at the common ground, C_{p1}, had a peak value of 150A, of which 120A flowed the ground wire, C_{p4}. The current flowing the ground wire produced a significant voltage drop across the impedance, V_{p6}. Then, voltage across the capacitance, V_{p6}-V_{p7}, was as large as 1000V. Between the hot and return ends of the bypass diodes, the surge voltage, V_{p8}, was between +120V and –40V and oscillated with a few MHz. Among more than 100 measured waveforms, the maximum value of the surge voltage was +180V/-140V. Because voltage between the hot and return ends is divided by the six diodes

connected in series, each diode can withstand this level of surge voltage. We need to study, however, influence of the surge voltage on other power devices such as shunt transistors.

VII. ESD tests for situation over the South Pole

To test the situation over the South Pole, we used low-temperature plasma environment, because the solar paddle back surface is facing to the ram direction where dense ionospheric plasma exists. A coupon was placed inside a vacuum chamber filled with Ar plasma. The coupon was biased to a negative potential by an external circuit as shown in Figs. 8 and 9.

First, we tested the nominal condition where the satellite has a negative potential nearly equal to the solar array generating voltage with respect to the plasma. We biased a coupon to -60V and exposed it to Ar plasma of 1eV temperature and $5 \times 10^{11} m^{-3}$ density for 65 minutes corresponding to power generation time in orbit. We carried out this test twice but observed no arc. Therefore, under the nominal condition, there would be no primary arc on the solar paddle back surface. When the aurora electron current density is high, however, the satellite potential may drop to a negative value as it was observed for DMSP and Freja. Because the Ag-TF insulator surface is faced to the ram direction, its surface potential can be assumed to near zero potential as it accumulates ion positive charge.

We looked for the threshold of primary arc inception. We biased the coupon to a negative potential until we observed a primary arc on the surface. At each biased voltage, we waited for 20 minutes assuming the worst case where ALOS stays in the aurora zone for the longest time. We observed primary arcs at -90V but not at -80V. Therefore, the threshold is between -80 and -90V. Arcs were observed on CFRP surface. CFRP surface is made of conductive fiber and synthetic resin that is insulator. Therefore there are numerous triple junctions all over the exposed CFRP surface.

Because there is only 20V margin between the arc inception and the nominal condition, we need to verify primary arcs on the paddle back surface does not cause any damage to the power circuit. We did the tests similar to the ones carried out for the North Pole situation, i.e., secondary arc and surge voltage. Before that, we need to estimate how many primary arcs would occur in orbit. Because we have no three-dimensional charging analysis software that can accurately calculate charging potential of a polar orbiting satellite, we rely on a simple analytic method.

Total negative current collected by ALOS is given by

$$I_- = j_a A_{cst} + j_a A_{pcf} + j_a A_{pcb} = a \times 1.5 \times 10^{-6} (A) \qquad (9)$$

where A_{cst}, A_{pcf} and A_{pcb} are total conductive area on the satellite body, exposed conductive area such as interconnector on the paddle front surface and exposed conductive area on the paddle back surface, respectively.

They are A_{cst}=45m^2, A_{pcf}=0.5m^2 and A_{pcb}=1m^2. Total positive current collected is given by

$$I_+ = c(\phi_{sat}) \left[j_i A_{csr} + j_i A_p + j_{phk} (A_{st} - A_{csr}) \right] \approx c \times 0.002 (A) \qquad (10)$$

where A_{csr} and A_p are conductive area on the satellite body facing the ram direction and solar paddle area.

We assume A_{csr}=20m^2 and A_p=66m^2. We neglect contribution due to photo-electron current because photo-electron current of Black Kapton is j_{phk}=7.2x10^{-6}A/m^2 [15] and makes only 0.3mA in total. The factor c accounts for expansion of ion collecting sheath from the satellite body and solar paddle. At the nominal condition of ϕ_{sat}=-60V, we cannot expect large expansion of the sheath considering the size of ALOS. Therefore, we approximate c as unity. When I_- exceeds I_+, the satellite body potential ϕ_{sat} becomes further negative. This occurs when

$$a > \frac{0.002}{1.5 \times 10^{-6}} = 1300 \qquad (11)$$

When the aurora current density becomes 1,300 times the nominal value, the satellite experiences negative charging. This rarely occurs. Only once in a year or so according to the analysis discussed in the previous section, but still possible during the five-year mission time of ALOS. When ALOS encounters such a severe environment, the satellite body potential quickly becomes further negative and the dielectric material on the paddle back surface acquires positive charge from the incoming ions. Assuming that the capacitance of synthetic resin on CFRP surface to be of the order of 10^{-7} F/m^2 and the ion ram current density of the order of 10^{-5}A/m^2, it takes one second to charge the dielectric material to 100V. Assuming ALOS stays 1200s in the aurora zone (the worst case), the expected number of arcs is 1200. Dividing the number of arcs by the number of circuits, 72, we obtain 17 as a reference value used for the ESD tests. Considering uncertainty associated with assumed numbers, the number of arcs may vary with several orders of magnitude.

We carried out the test against sustained arc twice using two different coupons. For each case, we had 500 primary arcs and observed no secondary arcs. Considering the reference value, 17, the total 1000 arcs gives sufficient margin. In Fig. 24 we show the arc positions identified during the secondary arc test. Many arcs were observed on CFRP surface around the coupon edge where Ag-TF insulator film was not placed. Arcs were also observed at the edge of Ag-TF film where narrow gap of CFRP is exposed. Some of the arcs identified at the middle of Ag-TF film are misplacement, which occurred because the computer software misinterpreted the reflection at the surface as a part of the optical flash associated with primary arcs. We also observed arcs around and on the diode board. The diode board has triple junction made of white insulation coating and exposed metallic legs of the diodes. Although some of arcs directly hit the diode, they showed no sign of degradation when we measured the forward voltage of each diode before and after the test.

For each coupon we tested against the secondary arcs, we also carried out the test for the surge voltage. Again, we had 500 primary arcs for each coupon. When primary arc occurred the surge voltage that was mainly monitored at V_{p1} in Fig. 9 showed little disturbance for most of the cases. The voltage amplitude was typically less than a few volts. When a primary arc occurred on the diode board and the arc current flows through HOT line, however, there was a surge voltage as large as 20V between the strings as shown in Fig.25. This is the voltage that appears across the power control circuit elements at the event of primary arc. The number of this type of arc was 6 against total 500 arcs. Figure 26 shows the positions of those arcs. All of them were direct hit to the diodes.

Repeated primary arcs on CFRP surface caused noticeable damage on the surface. Figure 27 shows an example of damage found on CFRP. CFRP fiber was broken and we observed hangnails. Care must be taken to avoid protruded carbon fibers from damaging wire insulation jacket of power harness.

VIII. Design Modification and Extreme Test

The analyses and laboratory experiments shown in the previous sections demonstrated that the baseline paddle design was susceptible to back surface charging and arcs. Although the baseline design proved its immunity to sustained arc and tolerance to expected arc accumulation, we explored potential modifications to the baseline design in order to mitigate charging and arcing and to improve the paddle's robustness [6].

Referred to the design guidelines [16]-[18], we apply the following basic guideline in devising the paddle's modifications:

- To ground floating conductors for preventing potential differences,

- To encapsulate floating or high-voltage conductors which are exposed to space, and

- To apply conductive coating to exposed insulator surface.

Although the uncompromising application of this guideline is desirable, the modifications are subject to realistic constraints. The paddle's proto-flight model was once already manufactured, qualified, and assembled to ALOS prior to the ADEOS-II accident. A number of ideal modification candidates have brought technical difficulties, schedule problems, and/or additional risks, and therefore, we were not at liberty to adopt them. For the back side of the solar panels, the best and ideal way to mitigate the charging is: (1) to replace the Ag-TF thermal films with conductively coated Ag-TF thermal films and to attach them to the substrates with conductive adhesives, and (2) to remove the bypass diode boards from the back side and to implement solar cells with integrated bypass function (IBF) to the face side. This ideal approach, however, were not acceptable, because the removal of the Ag-TF films and solar cells was not feasible and it would inevitably require re-manufacturing of the whole panels.

Because Ag-TF film is not grounded small arcs would occur once the Teflon surface acquires a negative potential of –1500V that is likely when the aurora electron current density increases by a factor 100 from the nominal value. Even if each arc is small, repeated arcs may degrade the Teflon film as their effects accumulate, or may induce signal noises and operation disturbances for on-board components. To avoid such degradation and disturbance, we considered increasing the arc inception threshold from –1500V by grounding the silver layer. We pasted conductive paint along four edges of Ag-TF film so that the silver layer partially exposed at the edges is connected to CFRP surface as shown in Fig.28.

The conductive paint has been extended to cover any exposed CFRP surface as much as possible. There are two purposes for this practice. The first one is to limit the arc current to the panel ground line, which causes large surge voltage as shown in Fig.23, by inserting additional resistance of the order of MΩ between the arc plasma and the panel ground line. The second one is to hide the numerous triple junctions of CFRP by the conductive material so that we can increase arc inception threshold in plasma environment over the South Pole.

Minimizing arc occurrence at the edge of Ag-TF and CFRP surface, however, gives an undesirable side effect that arcs now tend to occur over the diode boards. We like to avoid direct hit of arcs to the diode boards because the diodes are indeed what we are protecting from the arcs. To give additional protection to the diode, we decided to cover diode board by insulating film as shown in Fig. 29. In this way, we can suppress arc inception at the diode board. Also we can protect the diode board from being involved with surface flashover originated from other parts of the solar paddle. In addition, we have grounded the heat sink of the diode board to the panel structure via the

conductive adhesive that gives resistance of the order of 100kΩ. We have also given extra insulator coating to diode end caps that are facing each other with 40V potential difference.

Figure 30 shows a photograph of the mitigation design. We call this design as mitigation design. We have tested this coupon extensively so that there would be no unforeseen side effects hidden in the design. Table 6 lists the comparison of the arc inception threshold between the baseline coupon shown in Fig.4 and the mitigation coupon shown in Fig.30. The arc inception threshold increased especially for the situation over the South Pole where the coupons were tested under plasma environment. Because numerous triple junction of CFRP are now hidden from the plasma, the next triple junctions available for arcing are the border between harness and conductive adhesive covering CFRP. For the situation over North Pole where the coupons were tested under electron beam irradiation, small arcs previously observed at the edges of Ag-TF film did not occur as the silver layer is now grounded. Small arcs occurred at the triple junction between harness and the conductive adhesive only after voltage as large as -8000V builds up.

The threshold of surface flashover does not improve for the mitigation coupon. The film over the diode board, however, is very effective to limit the influence of surface flashover on the diode board and its circuit. Figure 31 shows a snap shot of the surface flashover taken via an IR video camera of 30 frames/s. The surface flashover plasma cannot enter the diode board as the film prevents its penetration. We had 2800 surface flashover on the mitigation coupon and observed none of them connected to the diode board. Needless to say that there was no secondary arc. The conductive adhesive over CFRP also limited the current to the panel ground (GND) line. For the case of baseline design, more than 40% of the current supplied by the external capacitance flowed through the GND line causing a large common mode noise. For the mitigation design, the current to the GND line was limited to less than 20% of the current supplied by the external current thanks to the additional resistance given by conductive adhesive.

The Kapton® film over the diode board may introduce two new problems: internal charging in the complex of the diode board and the Kapton® film, and temperature increase within the diode board and the neighboring area. The internal charging was experimentally studied and it did not show a threat.

The temperature increase was tested and analyzed. All the diode boards except those on the innermost panel stayed within acceptable temperature range. Thus, all the diode boards except those on the innermost panel are shielded by Kapton® films. The temperature increase may promote outgassing below the Kapton® film and may pose danger of Paschen-type discharge inside the film. We tested the possibility of Paschen-type discharge within the diode board inside a vacuum chamber where the background pressure was raised to give the optimum

condition for the Paschen-type discharge, 1Torr(=133Pa), with respect to the distance between the diodes, 14mm. We produced a small triggering plasma by focusing a YAG laser pulse of 20~80mJ between two diodes connected to a solar array simulator of 40V/2.7A to simulate a small primary arc caused by internal charging of the diode board insulator material. No secondary arc was observed after 300 triggering arcs. We raised the potential difference between the two diodes to 110V but observed no permanent sustained arc, though we observed temporary sustained arcs. Only after we raised the potential difference to 200V, we observed permanent sustained arc.

Finally, we carried out an extreme test to explore the maximum insulation strength of the final design. We used a coupon shown in Fig.33. The extreme test coupon already had nearly 3000 surface flashovers in the previous test where the diode board was not covered by the film to see the effect of conductive adhesive coating only. In the extreme test, we didn't also use the film because it was very difficult and too time-consuming to charge the diode board to a potential high enough to cause primary arcs by making energetic electrons penetrate the Kapton® film. We irradiated the diode board with 15keV electron beams of 100μA with more than 1mA/m^2 current density. The external circuit is shown in Fig.34. In the extreme test, we varied the voltage and current of the solar array simulator, V_1. For simplicity we used only one power supply between the two diodes facing with a distance of 14mm.

Table 7 lists the results of the extreme test. Secondary arcs were not observed until we raised the voltage to 110V. Because there was no secondary arc at 80V, the diode board design has the safety margin of more than a factor of two. At 110V, the maximum secondary arc duration was 60μs. Although we had a spherical electrode biased to -7000V and connected to a capacitor (160nF) to give additional energy (4J at most) to primary arc plasma, all the secondary arcs occurred even before the external capacitance began to discharge. At 150V, we observed permanent sustained arc between the substrate and the most positive diode. The arc was sustained for 6s until we turned off the power supplies. Because we expected sustained arc would occur between the two diodes, this result was rather unexpected. Figure 35 shows the photographs of the sustained arc location taken before and after the extreme test. The resistance between the diode leg shown in the figure and the panel ground was more than 30MΩ before the test and dropped to 38Ω after the extreme test. The photograph of the before-test clearly shows that a flake of conductive adhesive was accidentally bent toward the diode board circuit pattern. Although white coating insulated the circuit pattern, it was not perfect to suppress flashover. The distance between the tip of the conductive flake and the circuit pattern was only 0.7mm. We checked the photographs of perimeter of the diode board taken by a 60x microscope before the test and confirmed that the location shown in Fig. 35 had the

closest distance between the circuit pattern and the conductive adhesive. The result of the extreme test revealed unexpected weak points of the modified design, though it had enough safety margins. It was decided to take extra care when the conductive adhesive was painted around the diode board.

IX. Summary

As charging hazard on the ALOS solar paddle is addressed, electrostatic discharge (ESD) tests have been carried out to investigate charging and arcing phenomena on back surface of the solar paddle. In the present ESD tests, we have followed a procedure that has been adopted as the ESD test procedure in Japan based on our recent experience [19]. We first identified charging situations in orbit and determined the most appropriate test environment to simulate the charging situations. Then threshold of primary arc inception was found experimentally. We carried out numerical simulations to identify environmental parameters to produce the threshold condition and estimated the expected number of primary arcs in orbit. The number served as a reference value when we tested against secondary arc and surge voltage by repeatedly causing primary arcs on test coupons.

As ALOS passes the aurora zone near the North Pole, insulator at the backside of the solar paddle can be charged to a negative potential higher than 1000V because ionospheric ions cannot neutralize negative charge accumulated by aurora electrons because of plasma wake developed behind the solar paddle. Because ALOS stays as long as 1200s inside the aurora zone, the negative charging potential can reach over -8000V as the aurora flux increases. Because the satellite body is kept to plasma potential, so-called normal potential gradient occurs on the back surface, where insulator surface is more negative than nearby conductor.

We tested coupon panels that represent the baseline design of back surface of solar paddle in a vacuum chamber and irradiated the coupons by an electron beam. At the backside of the solar paddle, there were bypass diode boards that had exposed conductor connected to the solar array string circuit. A small arc was observed once the insulator surface potential became –1500V, though its current was too small to cause any effect on the power circuit except minor electromagnetic interference. As the surface potential became –7000V, we observed extensive surface flashover whose optical flash covered extensive area of the coupon panel.

When the surface flashover occurred the voltage across the diodes fluctuated indicating inception of temporary sustained arc that momentarily short-circuited the hot and return ends of the power circuit, though the duration was less than 10µs. The total number of surface flashover arcs accumulated exceeded 1000. We never observed permanent sustained arc nor temporary sustained arc longer than 10µs. Therefore, the diode board has the minimum insulation strength against secondary arc.

When the surface flashover occurred toward the CFRP surface, that was the panel ground, surge voltage of more than ±100V was observed between the hot and return ends. The surge voltage was developed by capacitance coupling between the ground wire line and solar array string circuit. As a large current flowed the ground wire, the voltage drop across the wire impedance, especially inductance, produced a large voltage across capacitance made of polyimide insulator and adhesive between the solar paddle ground and solar cells. Because the surge voltage will be divided by six diodes, probably it may not pose any threat to the diode board. Influences on other parts in the power circuit, such as a shunt transistor, should be considered carefully.

Not only the wake side, but also the ram side can have arcs once the aurora electron flux increases extremely high and the plasma density is very low so that the satellite body potential drops to a negative value. The body potential does not have to drop to a kV level to have arcs on the ram side. On the ram side, the insulator is charged by ionospheric ions. This is the inverted potential gradient case under LEO plasma environment. Near the South Pole, the ram side is the back surface and arcs occur on diode boards and CFRP surface. The threshold voltage for arc inception was found between -80 and -90V. Therefore, once the satellite body potential drops by 20V from the nominal value, -60V, arcs may occur on the ram side. We tested secondary arc and surge voltage under the situation over the South Pole. There was no sign of secondary arcs even when a primary arc occurred directly on the diode board. Surge voltage as large as 20V appeared between the strings when a primary arc directly hit the diode board. Repeated primary arcs on CFRP surface damaged CFRP and carbon fibers were protruded from the surface.

Although the baseline design proved to have enough strength against secondary arc and surge voltage, we modified the design to improve the paddle's robustness against arcing. We grounded silver layer of Ag-TF thermal insulator via conductive adhesive and extended the conductive adhesive to cover most of CFRP surface. This modification raised the threshold voltages for primary arc inception by more than a factor of 4 for both normal and inverted potential gradients. To prevent primary arc on the diode board and protect it from surface flashover originated elsewhere, the diode board was covered by thin insulator film. Extensive tests were carried out to check that the modification produced no undesired side effect.

Finally, we carried out a test under extremely harsh environment to find the limit of insulation strength of the diode board against secondary arc until the coupon broke down due to arcing. The results of the extreme test revealed unexpected weakness of the modified design though the modified design still had safety margin of more than 3 times the nominal condition. The flight design of the ALOS solar paddle has been finalized. In January 2006, ALOS was successfully launched and renamed as "Daichi", meaning the Earth in Japanese.

References

[1] S. Kawakita, H. Kusawake, M. Takahashi, H. Maejima, J. Kim, S. Hosoda, M. Cho, K. Toyoda and Y. Nozaki, "Sustained Arc between Primary Power Cables of a Satellite", *Proceedings of 2nd International Energy Conversion Engineering Conference*, Providence, AIAA 2004-5658, 2004.

[2] P. C. Anderson, "A Survey of Surface Charging Events on the DMSP Spacecraft in LEO", *Proceedings of 7th Spacecraft Charging Technology Conference*, ESA, SP476, 2001, pp.331-336.

[3] J. E. Wahlund, L. J. Wedin, T. Carrozi, A. I. Eriksson, B. Holback, L. Andersson and H. Laakso, "Analysis of Freja Charging Events: Statistical Occurrence of Charging Events", *ESA TECHNICAL NOTE*, SPEE-WP130-TN, 1999.

[4] J. Wang, P. Leung, H. Garret, and G. Murphy, "Multibody-Plasma Interactions: Charging in the Wake", *Journal of Spacecraft and Rockets,* Vol.31, No.5, 1994, pp.889-894.

[5] D. E. Hastings and H. Garrett, "Spacecraft-Environmental Interactions", *Cambridge Univ.Press*, New York, 1996.

[6] T. Iwata, T. Miura, Y. Nozaki, S. Hosoda and M. Cho, "Solar Array Paddle for the Advanced Land Observing Satellite (ALOS): Charging Mitigation and Verification", In *Proceedings DVD of 9th Spacecraft Charging Technology Conference*, 113iwa.pdf, JAXA-SP-05-001E, Tsukuba, Japan, April, 2005.

[7] M. Cho, R. Ramasamy, K. Toyoda, Y. Nozaki and M. Takahashi, "Laboratory Tests on Interaction between 110V Solar Arrays and Ion Thruster Plasma", *Journal of Spacecraft and Rocket*, Vol.40, No.2, pp.221-229, 2003.

[8]   M. Cho, R. Ramasamy, T. Matsumoto, K. Toyoda, Y. Nozaki and M. Takahashi, "Laboratory Tests on 110V Solar Arrays in a Simulated Geosynchronous Orbit Environment", Journal of Spacecraft and Rocket, Vol.40, No.2, pp.211-220, 2003.

[9]   I. Katz, V. A. Davis and D. B. Snyder, "Mechanism for Spacecraft Charging Initiated Destruction of Solar Arrays in GEO", *AIAA paper 98-1002*, January 1998.

[10] D. Payan, D. Schwander and J. P. Catani, "Risks of low voltage arcs sustained by the photovoltaic power of a satellite solar array during an electrostatic discharge: Solar Arrays Dynamic Simulator", *Proceedings of 7th Spacecraft Charging Technology Conference*, ESA, SP476, 2001, pp.151-162.

[11] M. Cho, R. Ramasamy, M. Hikita, K. Tanaka and S. Sasaki, "Plasma Response to Arcing in Ionospheric Plasma Environment: Laboratory Experiment", *Journal of Spacecraft and Rockets,* Vol.39, No.5, pp.392-399.

[12] http://nssdc.gsfc.nasa.gov/space/model/models/iri.html

[13] M. Cho and D. E. Hastings, "Dielectric Charging Processes and Arcing Rates of High Voltage Solar Arrays", *Journal of Spacecraft and Rockets,* Vol.28, No.6, 1991, pp.698-706

[14] H. Matsumoto, Private Communication

[15] M. Cho, S. Kawakita, M. Nakamura, M. Takahashi, T. Sato, Y. Nozaki, "Number of arcs estimated on solar array of a geostationary satellite", *Journal of Spacecraft and Rockets*, vol.42, No.4, pp.740-748, 2005

[16] D. C. Ferguson and G. B. Hillard, "Low Earth Orbit Spacecraft Charging Design Guidelines", *NASA TP-2003-212287*, February 2003.

[17] Carolyn K. Purvis, Henry B. Garrett, A.C. Whittlesey, N. John Stevens, "Design Guidelines for Assessing and Controlling Spacecraft Charging Effects", NASA TP-2361, 1984.

[18] European Cooperation for Space Standardization, "Spacecraft Charging - Environment-Induced Effects on the Electrostatic Behavior of Space Systems", ECSS-E-20-06 (Draft), 2004.

[19] M. Cho and T. Goka, "JAPANESE PRACTICES OF SOLAR ARRAY ESD GROUND TESTS", In *Proceedings DVD of 9th Spacecraft Charging Technology Conference*, 053_cho.pdf, JAXA-SP-05-001E, Tsukuba, Japan, April, 2005.
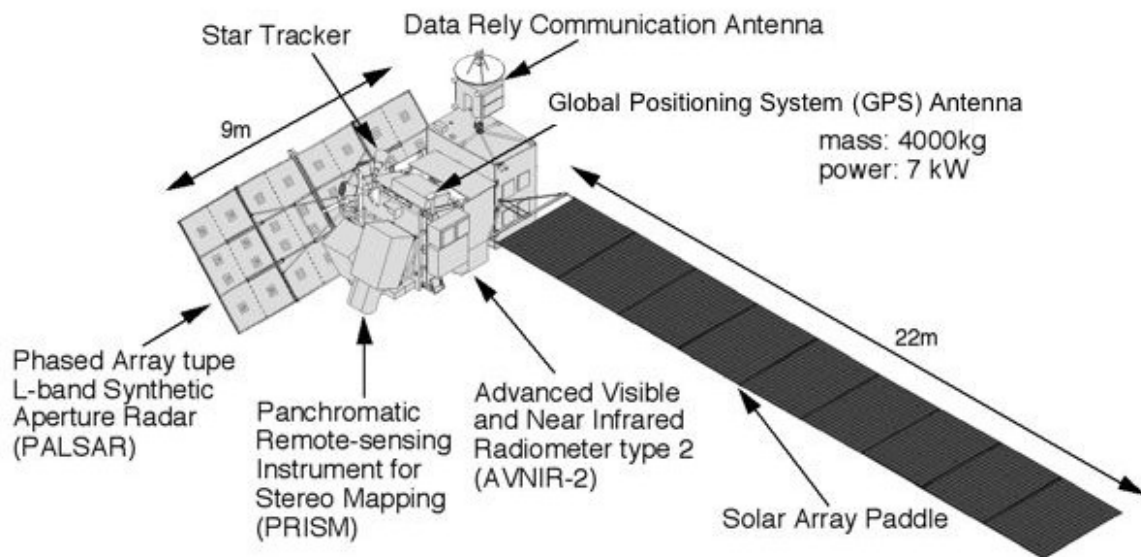
Figure 1. Illustration of ALOS in orbit
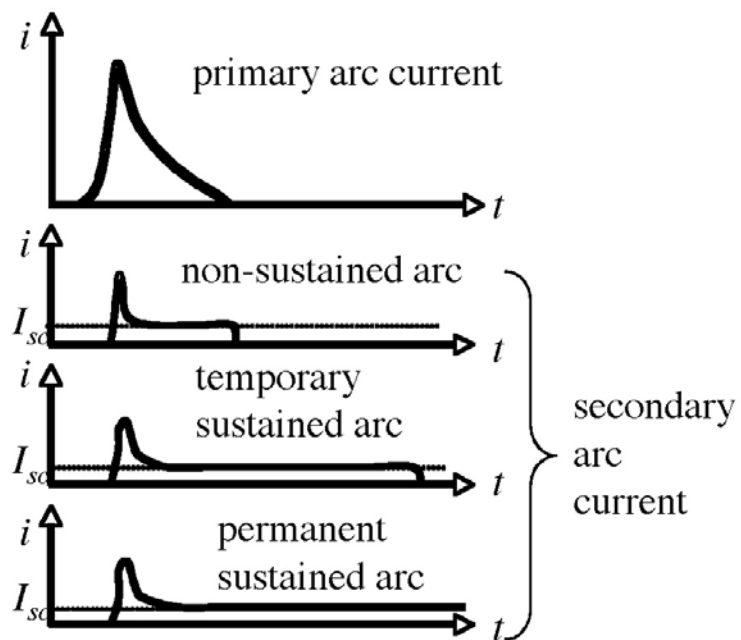
Figure 2: Definition of secondary arc current
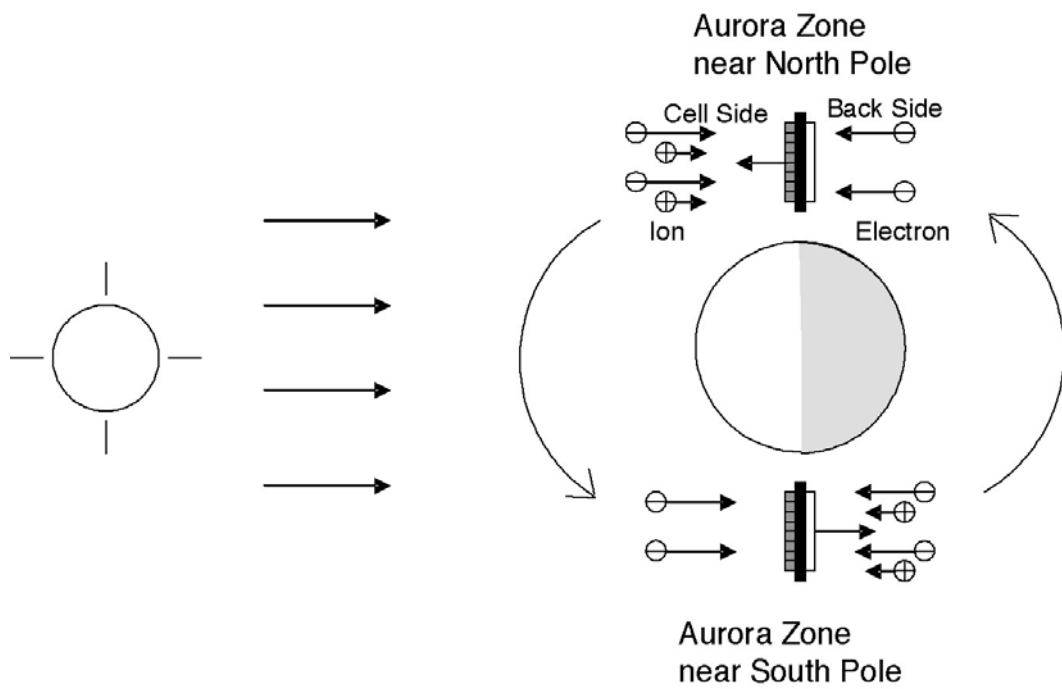
Figure 3. Schematic picture of ALOS solar panel direction in the polar orbit
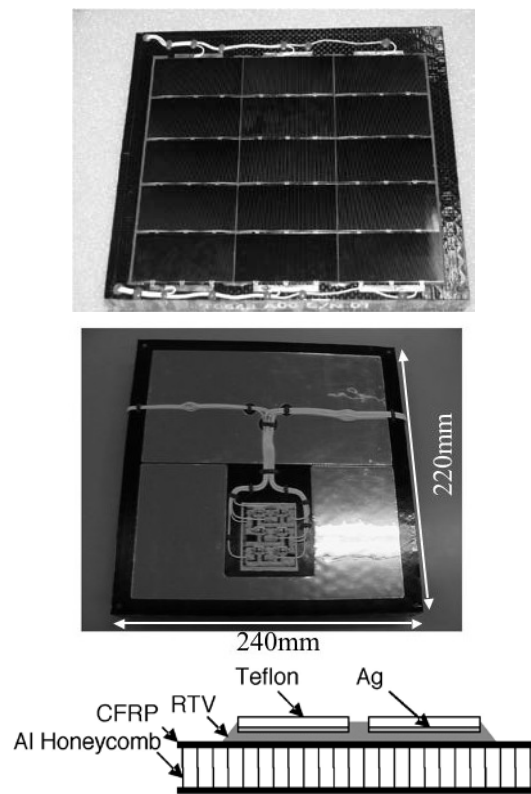
Figure 4. Photograph of ALOS solar panel coupon of the baseline design (Top: front side, Center: back side, Bottom: cross section).

Table 1: Possible severe surface charging situations of the ALOS solar paddle in polar orbit.

Orbit	Side	Direction	Potential gradient	Test environment
South Pole	Front	Wake	Normal	Electron beam
South Pole	Back	Ram	Inverted	Plasma
North Pole	Back	Wake	Normal	Electron beam
North Pole	Front	Ram	Inverted	Plasma
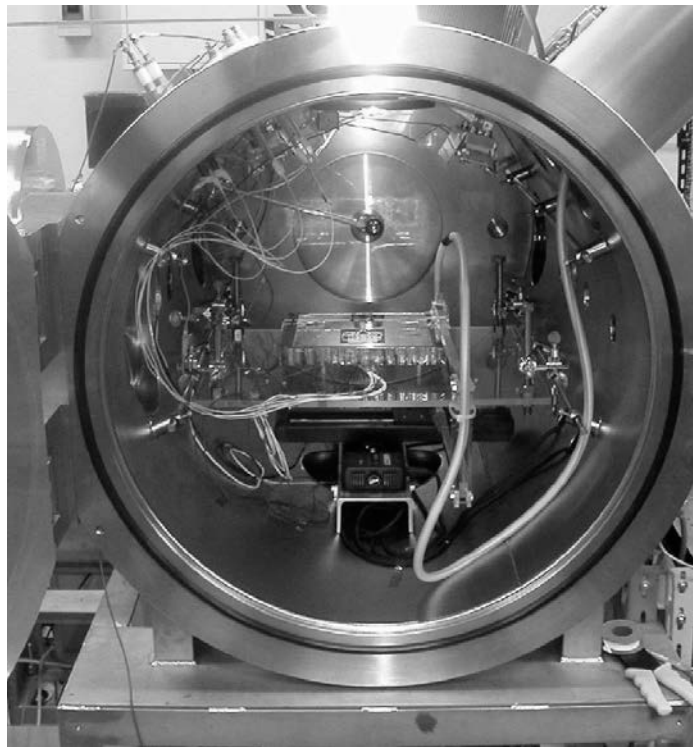
Figure 5: Photograph of a test coupon inside a vacuum chamber

Table 2: List of test cases and corresponding circuit diagrams.

Case No.	Purpose	Potential gradient	Test environment	Shunt	Circuit
1	Primary arc threshold	Normal	Electron beam	OFF	Fig.6
2	Secondary arc investigation	Normal	Electron beam	OFF	Fig.6
3	Surge voltage	Normal	Electron beam	ON	Fig.7
4	Primary arc threshold	Inverted	Plasma	OFF	Fig.8
5	Secondary arc investigation	Inverted	Plasma	OFF	Fig.8
6	Surge voltage	Inverted	Plasma	ON	Fig.9
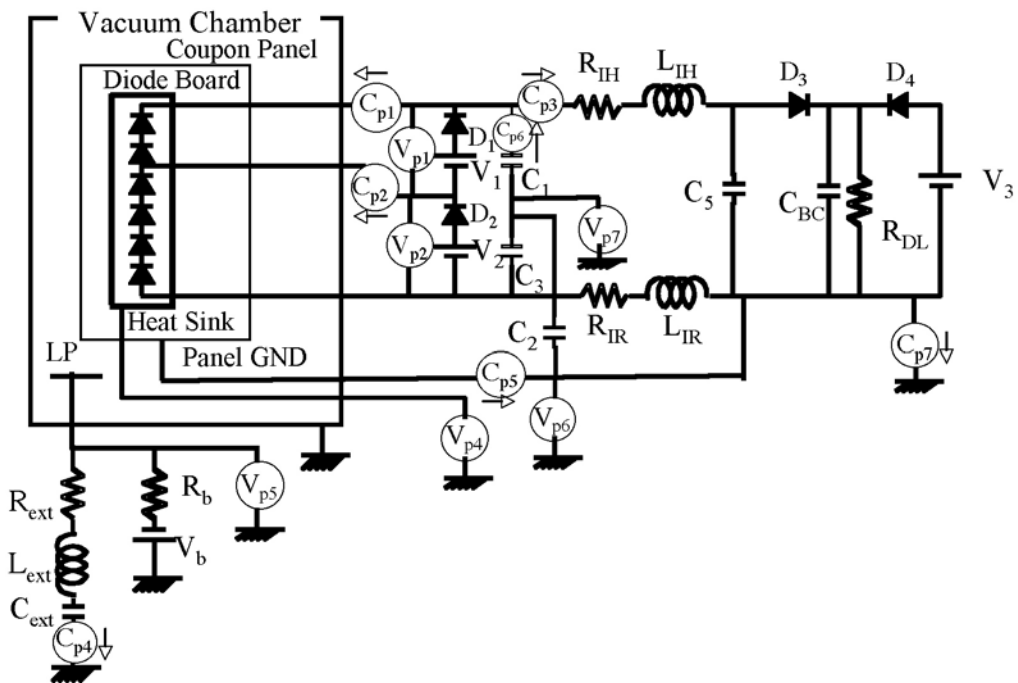
Figure 6: External circuit set-up for shunt-off configuration in electron beam test environment
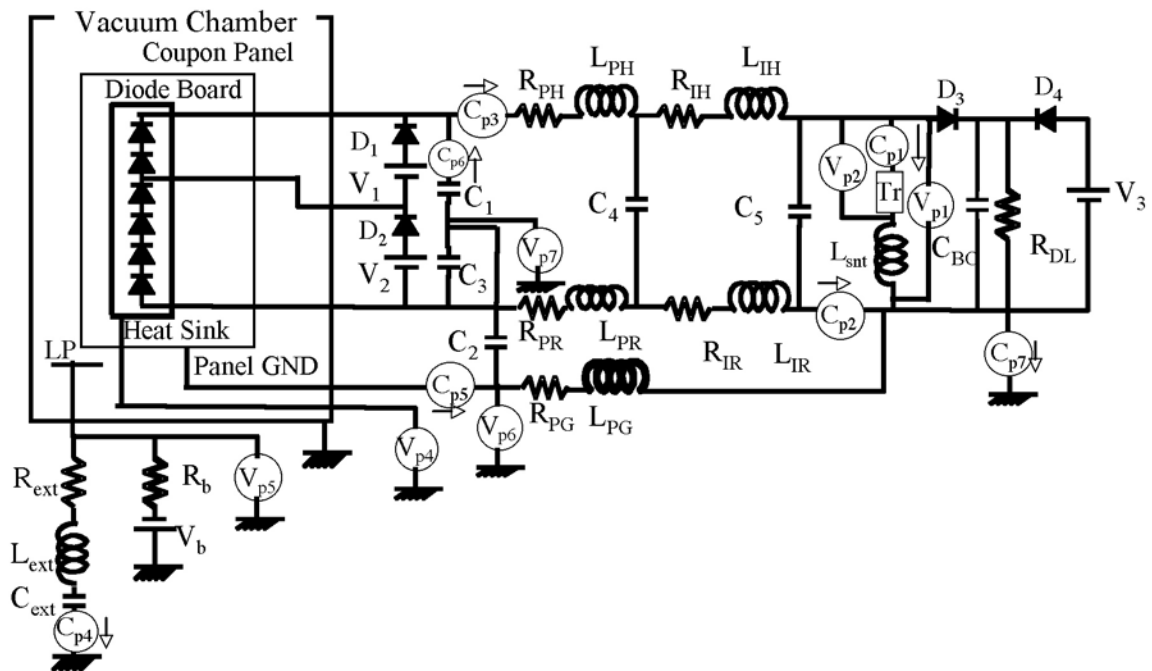
Figure 7: External circuit set-up for shunt-on configuration in electron beam test environment
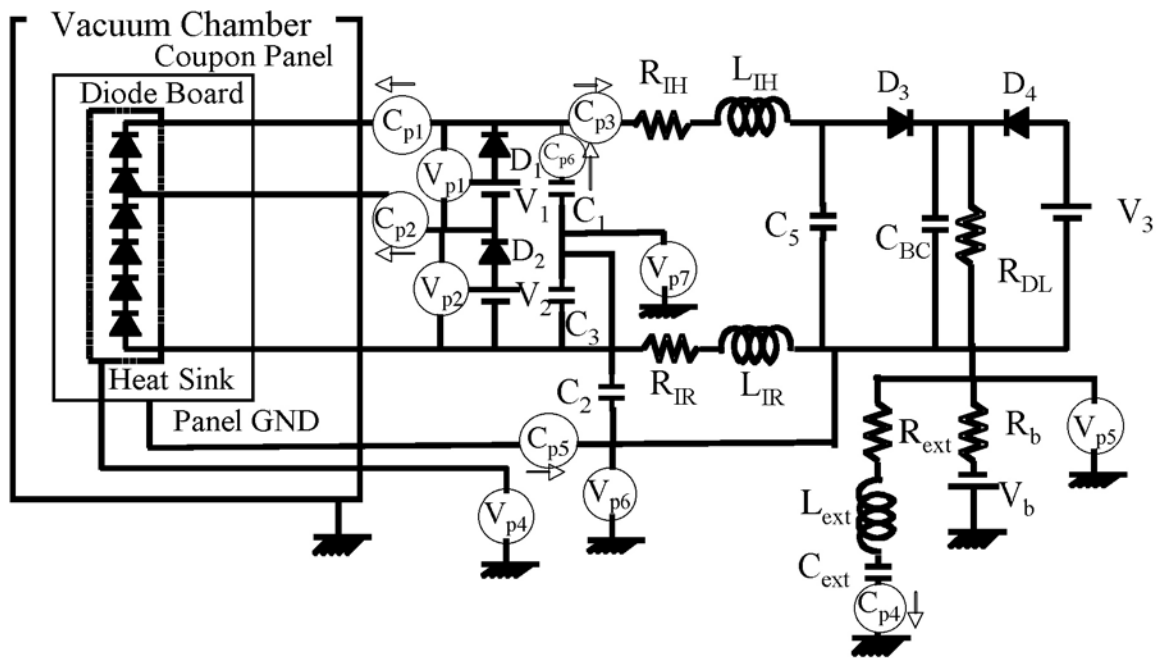
Figure 8: External circuit set-up for shunt-off configuration in plasma test environment
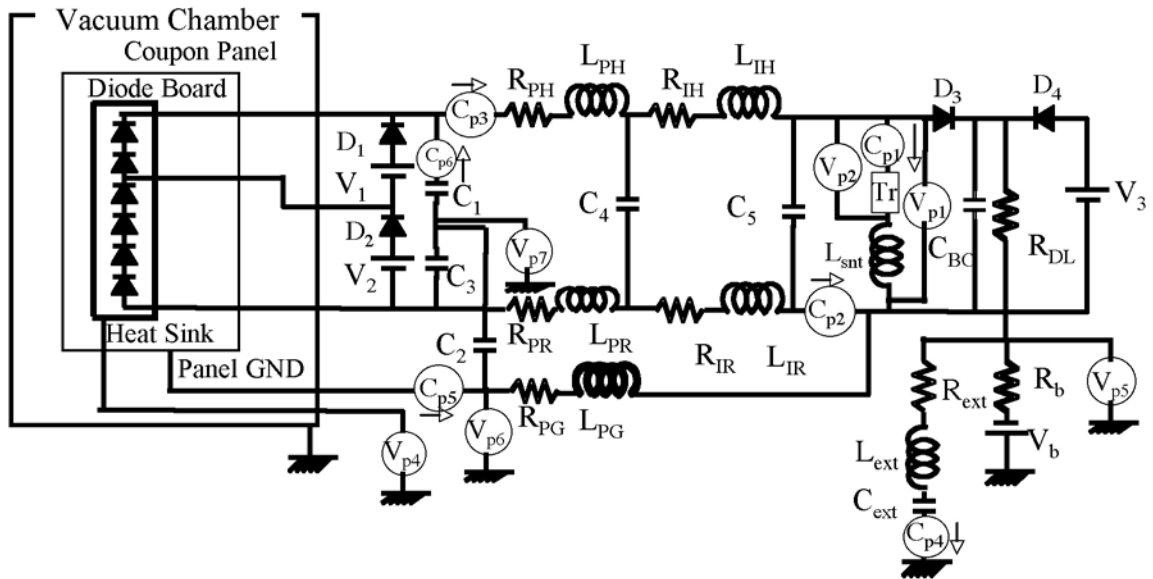
Figure 9: External circuit set-up for shunt-on configuration in plasma test environment
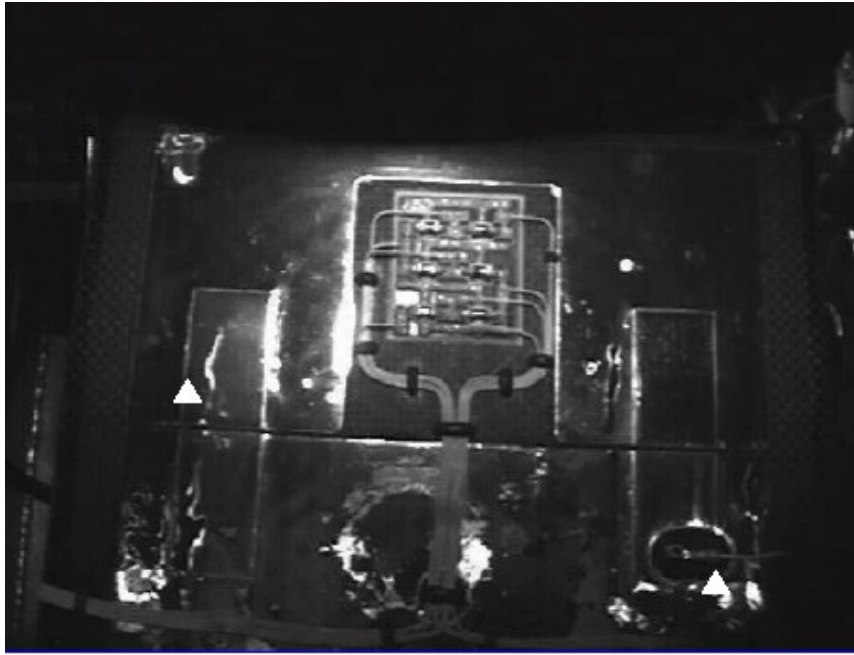
Figure 10. Positions of arcs (shown by white triangles) observed at 3keV electron beam energy.

Figure 11: Example of video image of surface flashover. This picture was taken when we irradiated the coupon with an electron beam of 15keV energy
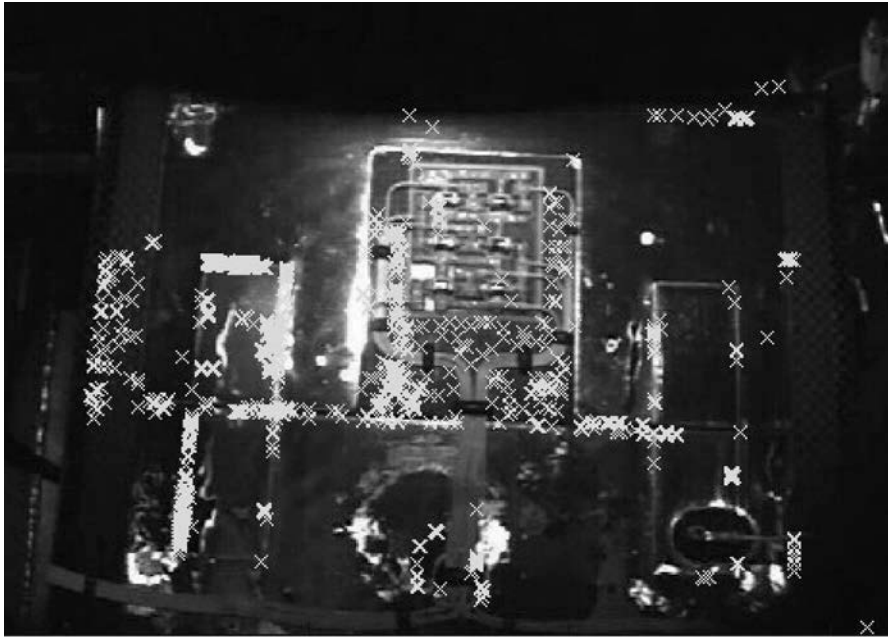
Figure 12. Arc positions observed for electron beam energy of 8keV.
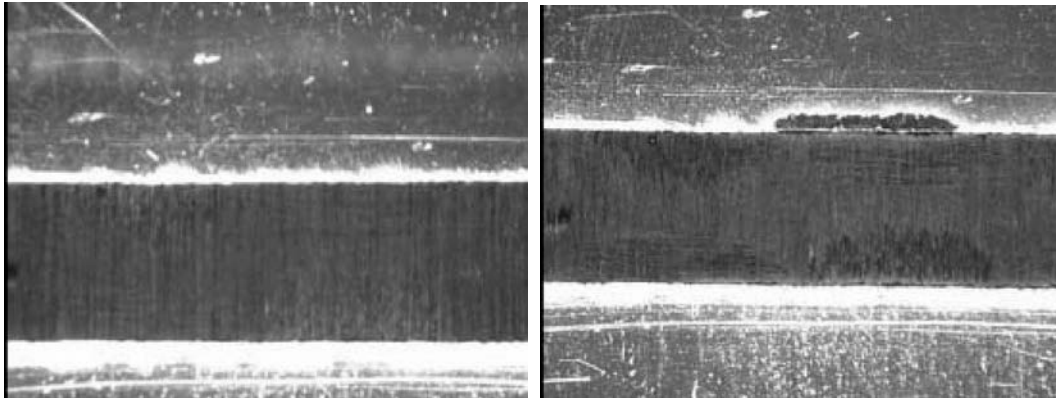
Figure 13. Photographs of Silver-Teflon edge before experiment (left) and after experiment (right)
The picture size is 3.6mm x 4.8mm
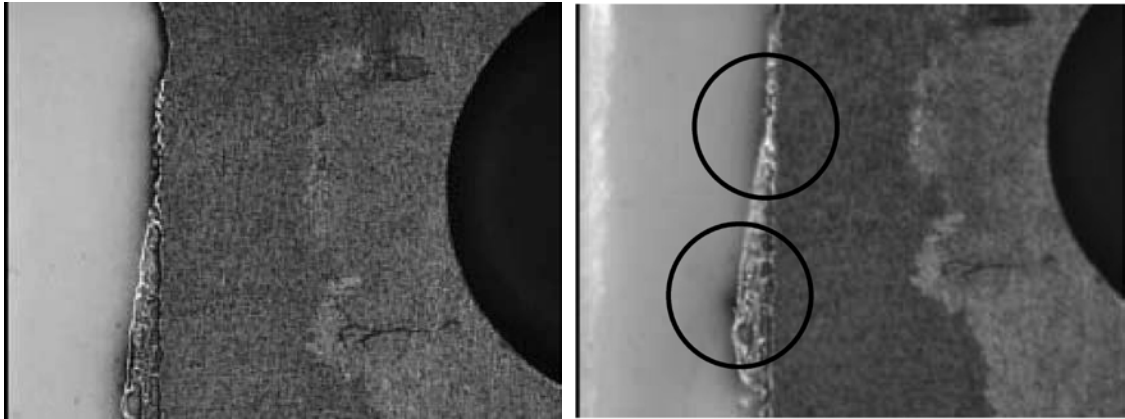
Figure 14. Photographs of diode board edge before experiment (left) and after experiment (right). Arc spots are surrounded by circles. The picture size is 3.6mm x 4.8mm
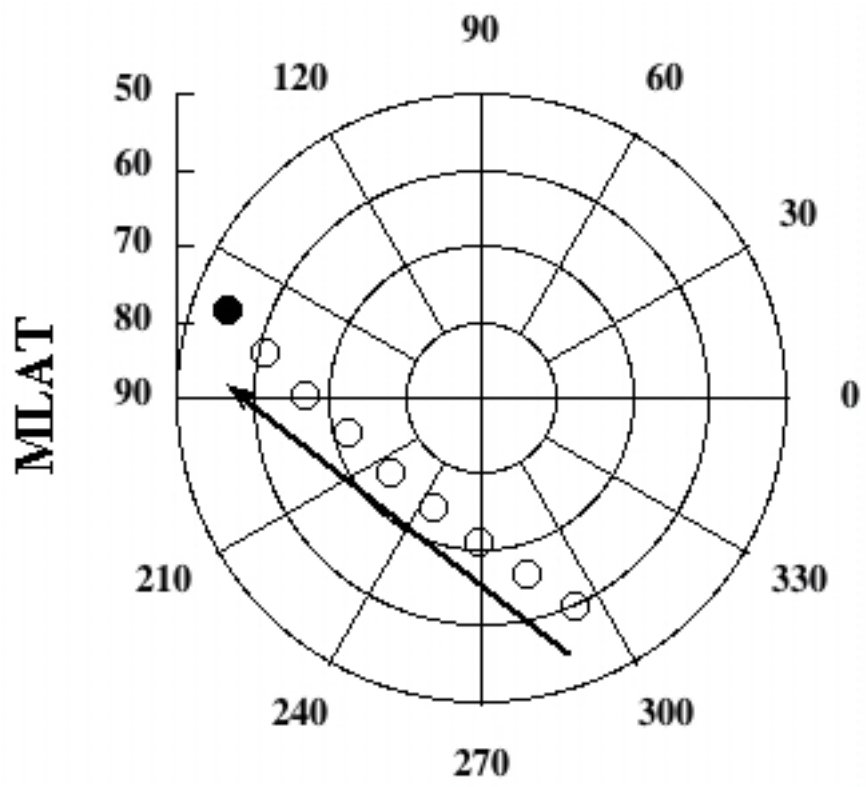
Figure 15. Trajectory of ALOS that flies the aurora zone over the North Pole for the longest time during night.

Table 3. Plasma parameters assumed for numerical simulation.

Plasma density	$2.0 \times 10^{10} m^{-3}$
Electron temperature	0.2eV
Ion temperature	0.2eV
Averaged ion mass number	13
Orbital velocity	7.2km/s
Nominal aurora current density	$3.2 \times 10^{-8} A/m^2$

20.48m

10.24m
or
20.48m

exposed conductor (-60V)

back & top surface:
insulator
$C=1.7x10^{-7}F/m^2$

plasma
flow
(7.2km/s)

3.08m

$\Delta x=0.02m$

7m   0.04m

front & bottom
surface:conductor (-60V)

boundary
potential
$\phi=0$
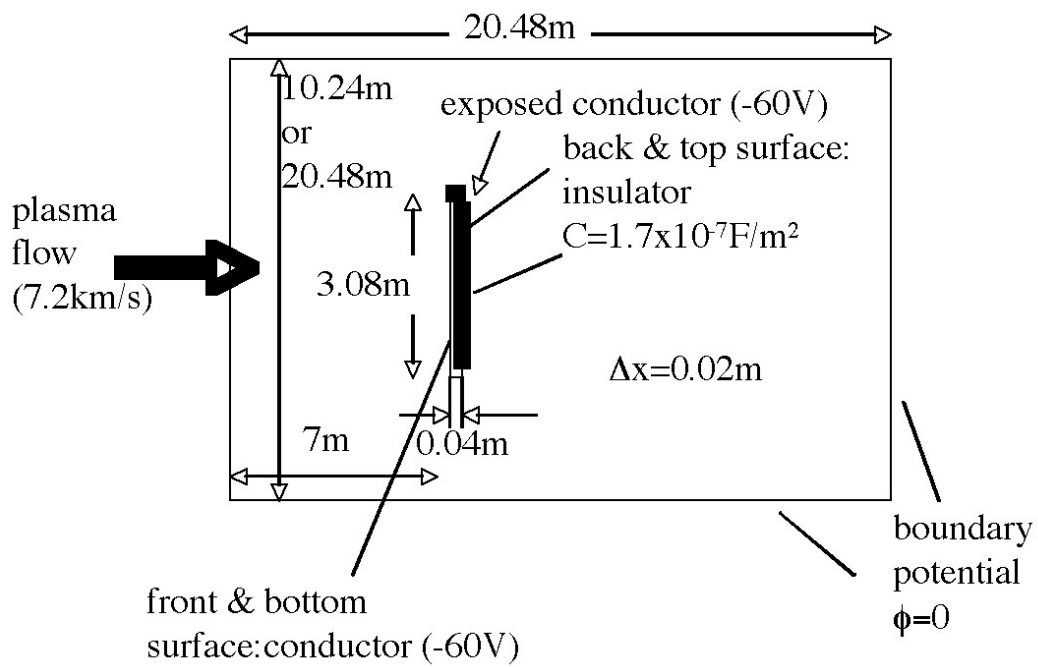
Figure 16: Schematic illustration of computational domain.

Table 4. Parameters of the numerical simulation cases.

Case No.	Charging time step, dt_L (s)	Total simulation time (s)	Aurora current density, j_a (A/m^2)	Aurora flux coefficient, a	Computational domain (m)
1	20	880	3.2×10^{-8}	1	20.48x10.24
2	40	1200	3.2×10^{-7}	10	20.48x10.24
3	8	408	1.6×10^{-6}	50	20.48x10.24
4	2	90	6.4×10^{-6}	200	20.48x10.24
5	1	180	1.6×10^{-5}	500	20.48x20.48
6	0.1	9	1.6×10^{-4}	5000	20.48x20.48
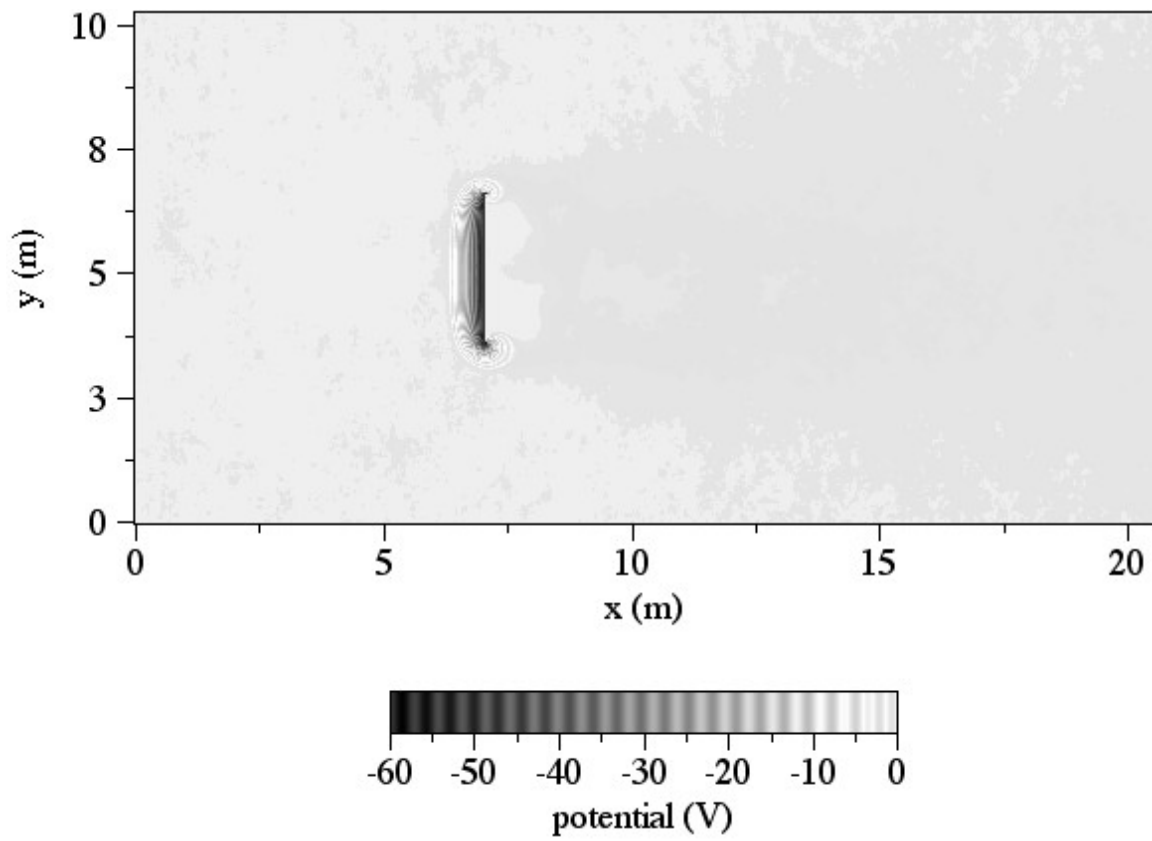
Figure 17. Simulation results of case 1 showing potential and ion density distribution at 880s.
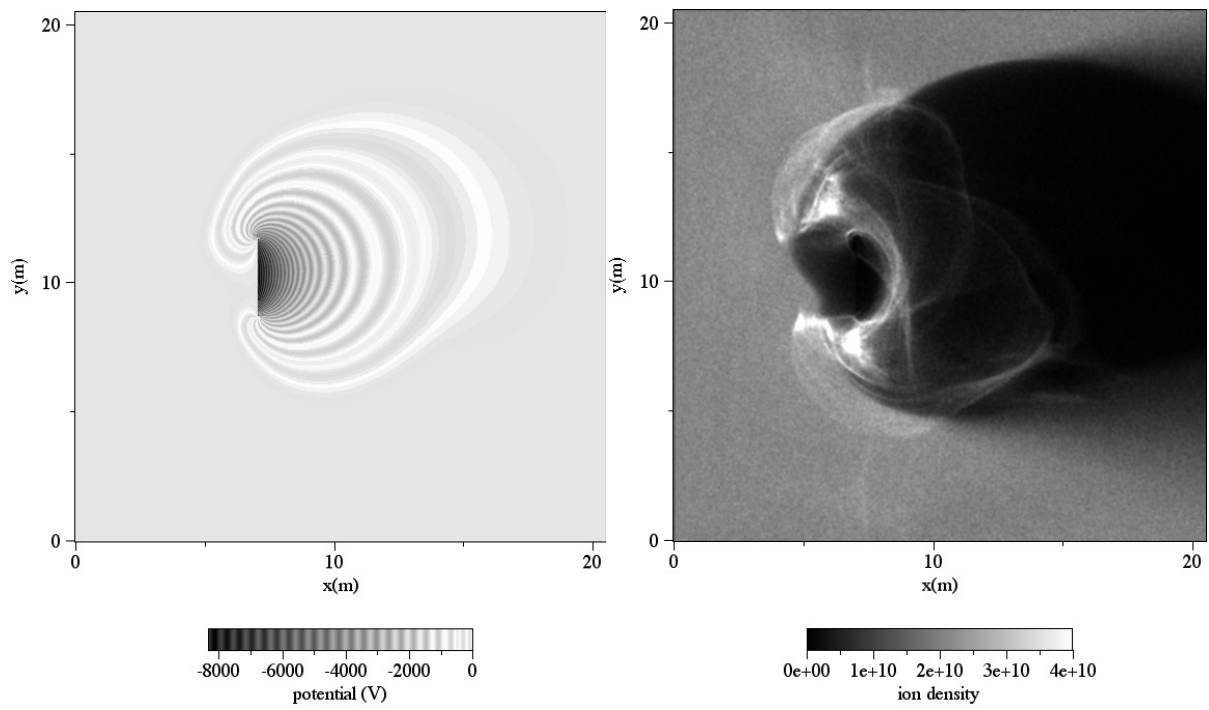
Figure 18. Simulation results of case 6 showing potential and ion density distribution at 9s.
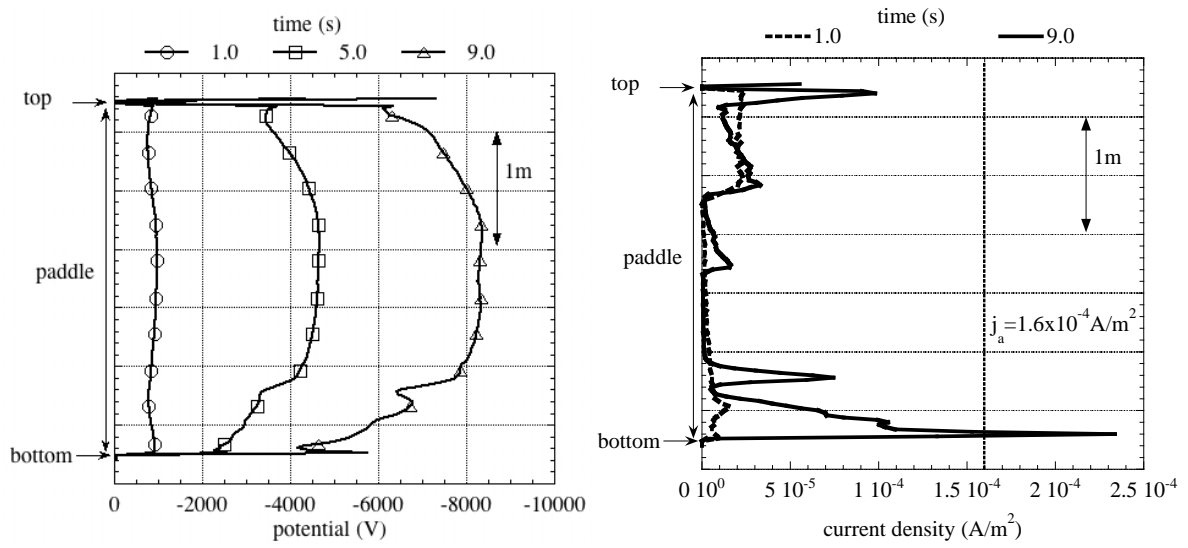
Figure 19. Simulation results of case 6 showing the ion current density and potential distributions over the back surface of solar paddle.
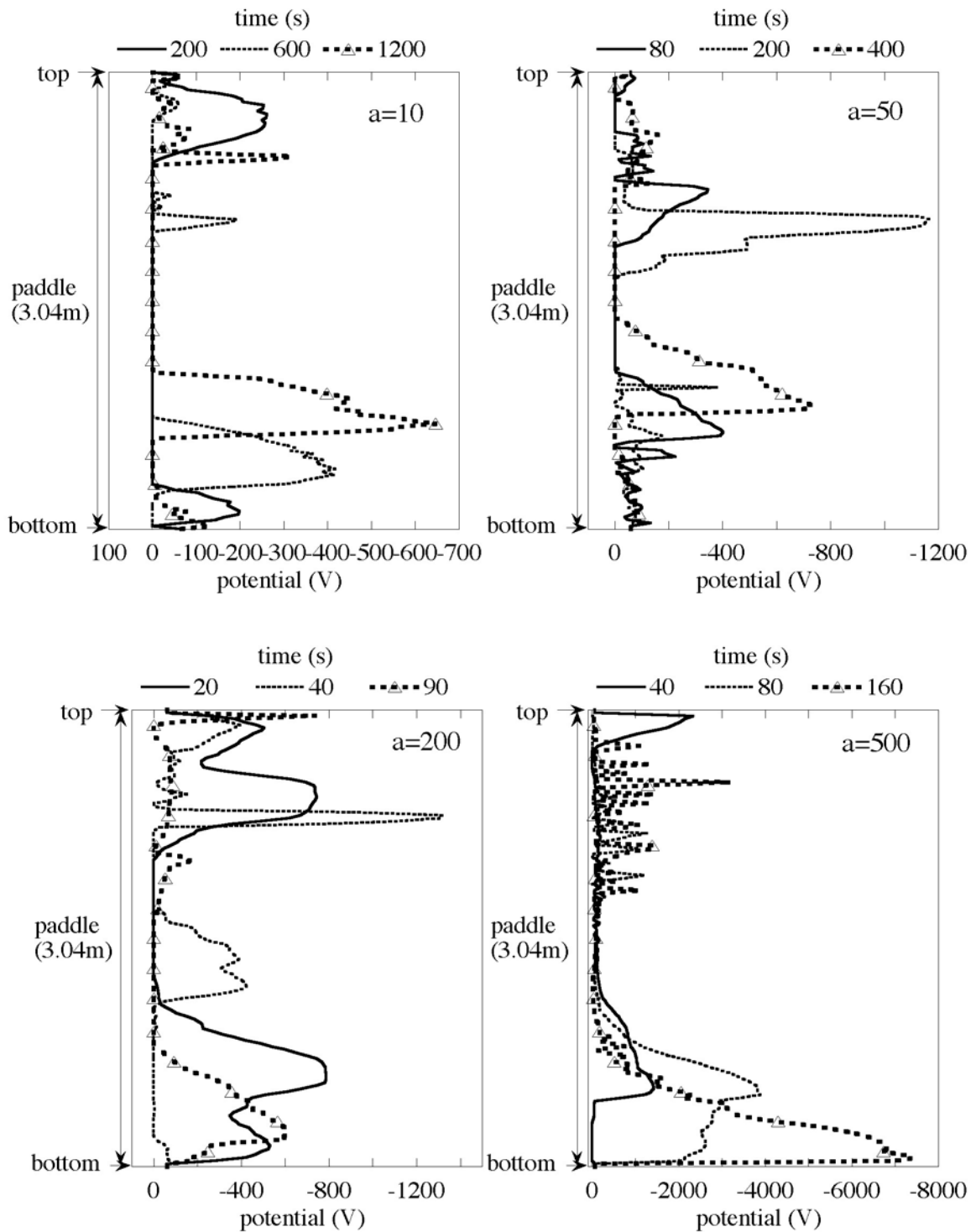
Figure 20. Temporal variation of paddle back surface potential for various cases of aurora flux coefficient. The vertical axis is measured from the bottom of the solar paddle with y=3.04m corresponding to the top of the solar paddle.
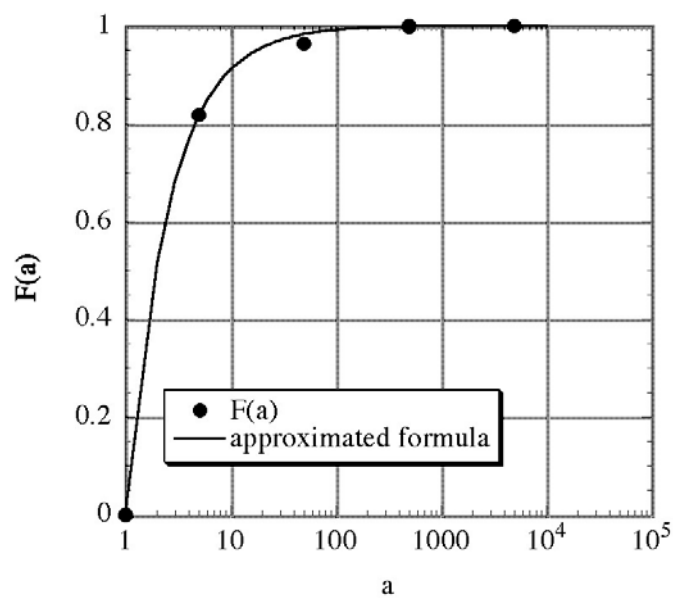
Figure 21. The probability of aurora flux coefficient. See the text for definition of *F(a)*.

Table 5. Frequency that a polar-orbit satellite encounters aurora flux higher than a given value

Electron flux over 1keV		Aurora flux coefficient, a	Frequency
$cm^{-2}s^{-1}sr^{-1}$	A/m^2		
$1.6x10^6$	$3.2x10^{-8}$	1	Nominal (steady)
$8.0x10^6$	$1.6x10^{-7}$	5	2000 events/year
$8.0x10^7$	$1.6x10^{-6}$	50	400 events/year
$8.0x10^8$	$1.6x10^{-5}$	500	A few times/year
$8.0x10^9$	$1.6x10^{-4}$	5000	Once in a few years
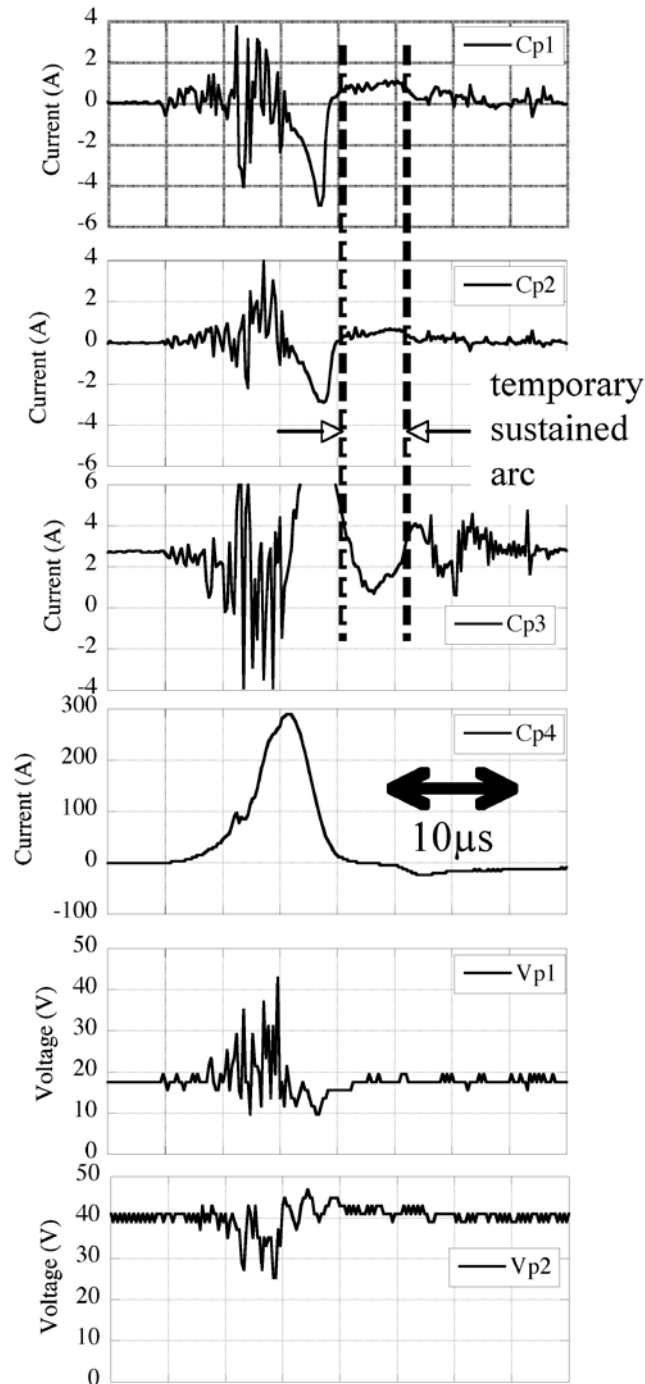
Figure 22. Typical waveforms when surface flashover absorbs charge stored in the external capacitance under the shunt-off condition. The arrow in the left figure indicates a temporary sustained arc.
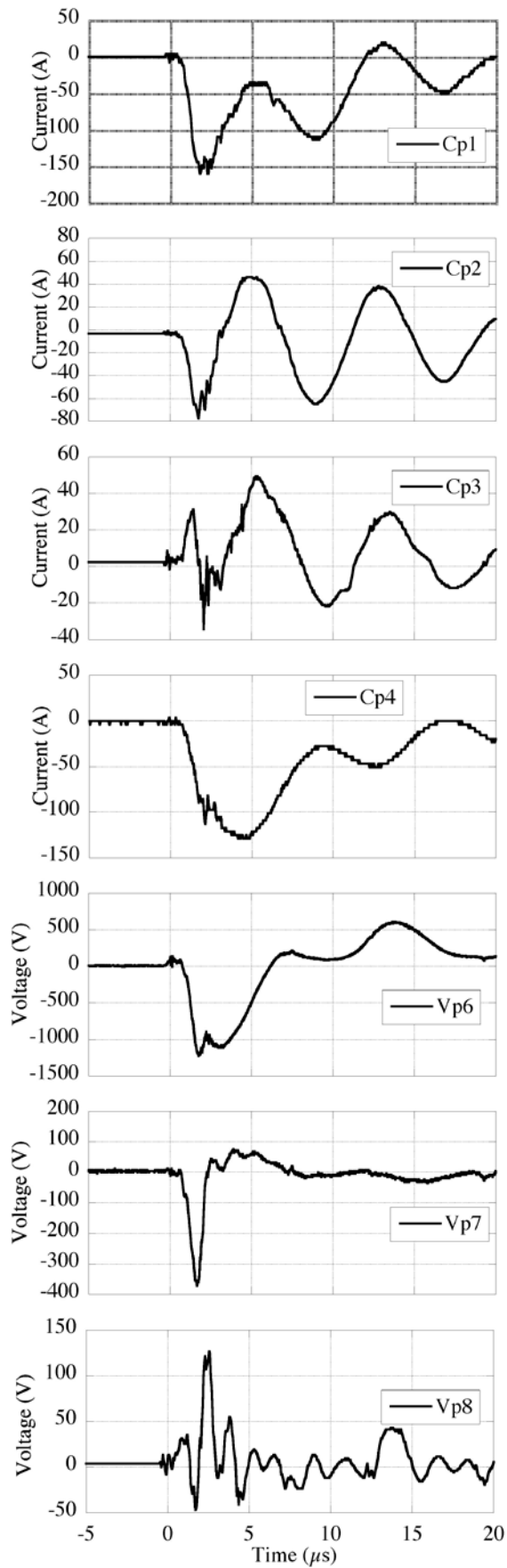
Figure 23. Typical waveforms when surface flashover absorbs charge stored in the external capacitance under shunt-on condition.
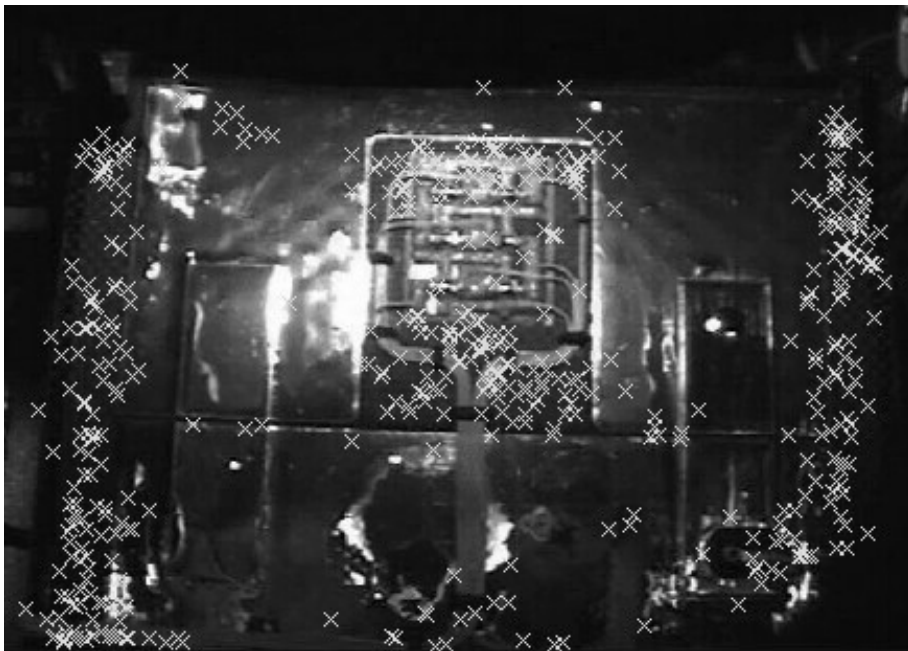
Figure 24: Arc position observed for case 5 (secondary arc in plasma) test.
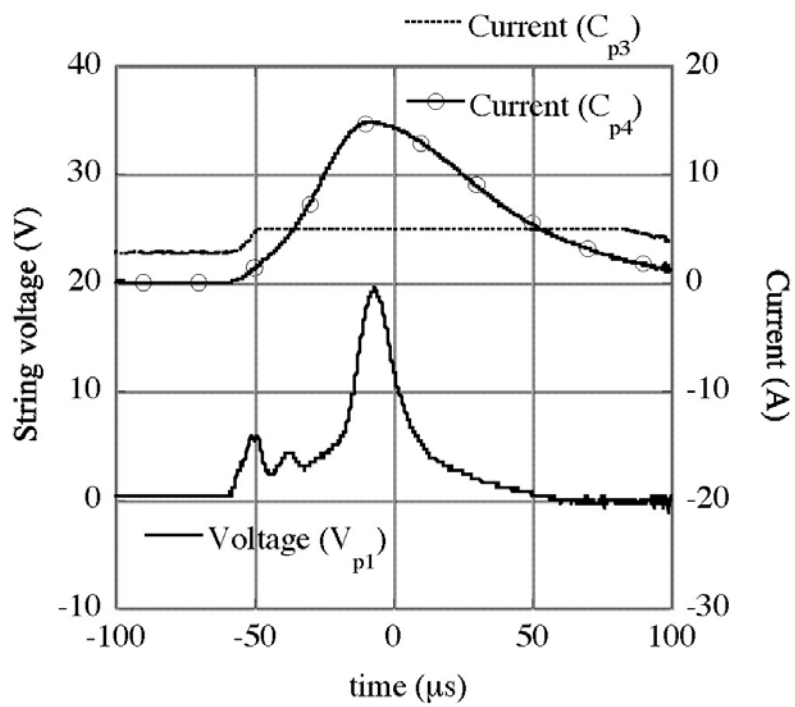
Figure 25: Arc current and surge voltage observed when a primary arc current flows through the HOT line. Note that the current measured by C_{p3} is out of range beyond 5A.
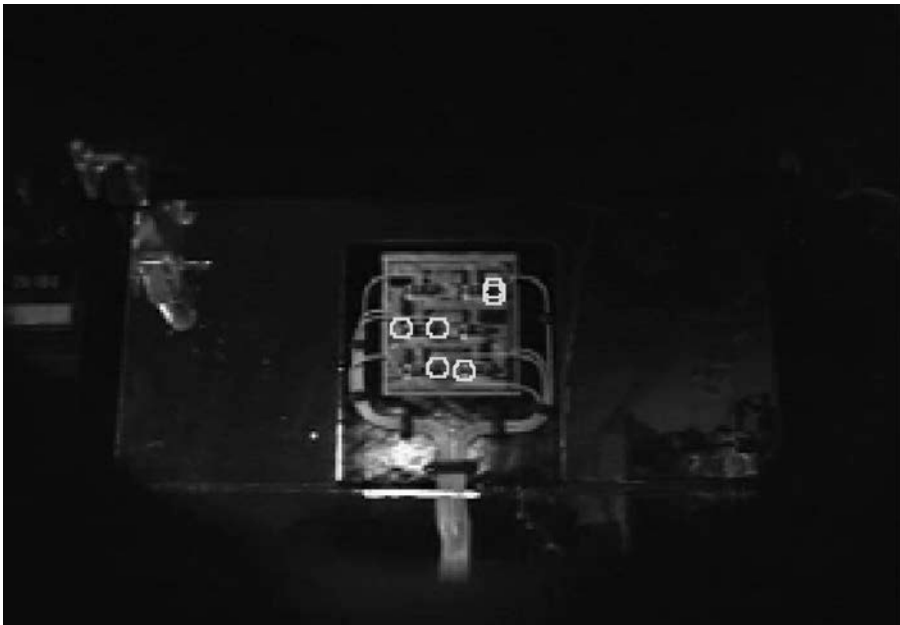
Figure 26: Position of primary arcs (white circle) that caused surge waveforms shown in Fig.25

Figure 27: Photograph of protruded carbon fibers from CFRP surface due to primary arcs in plasma environment. The size of photograph is 1.53mm x 1.14mm.
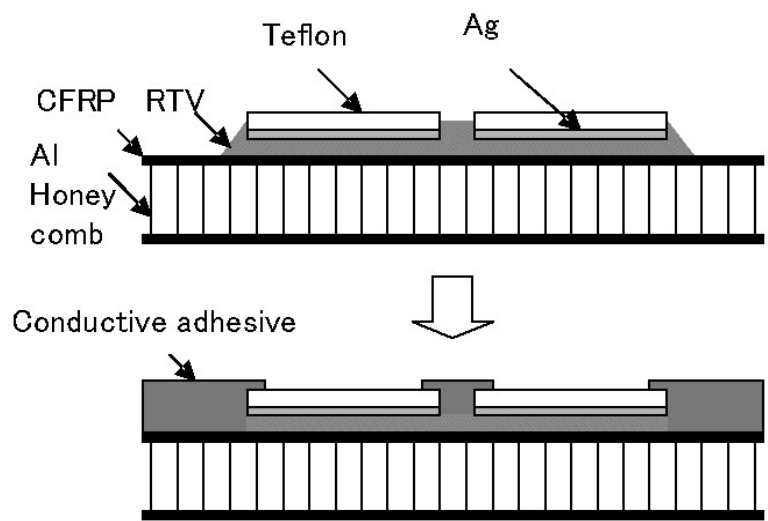
Figure 28: Conductive Adhesive Coating
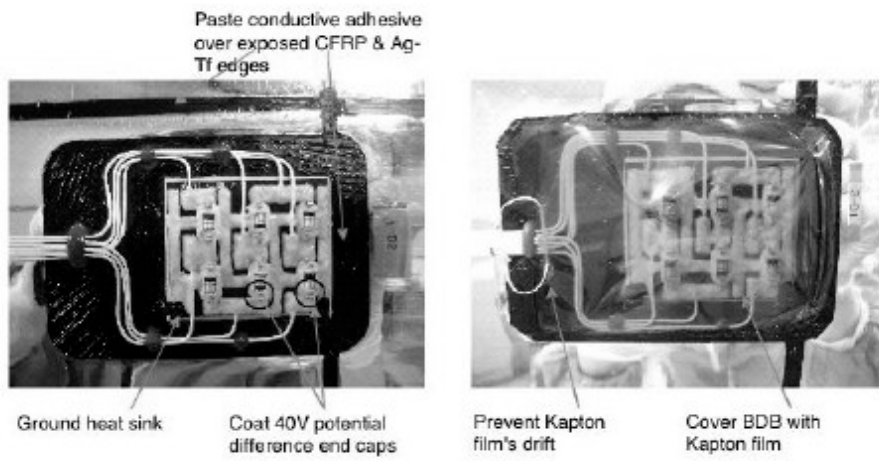
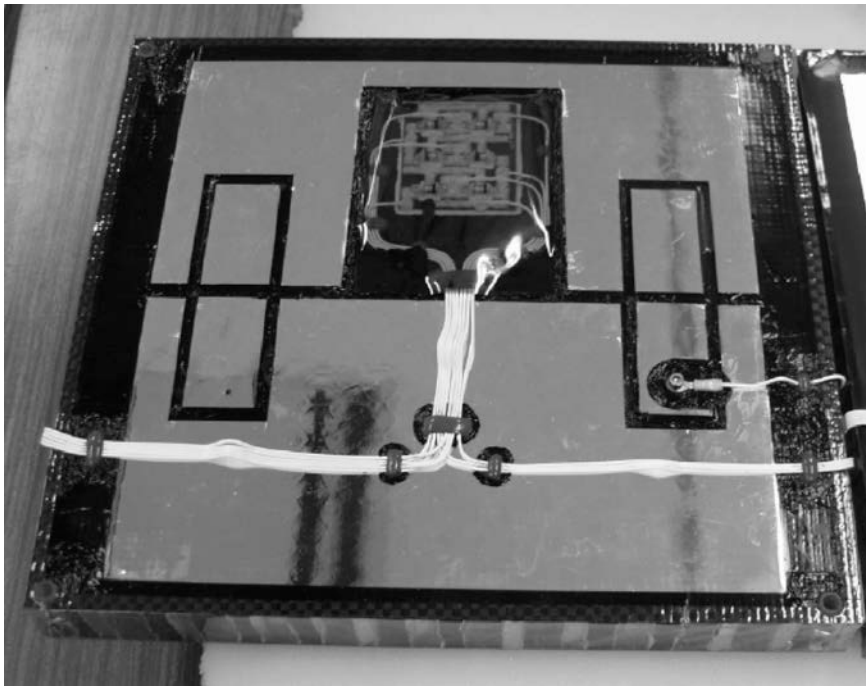Figure 29: Photograph of modified design of bypass diode board.

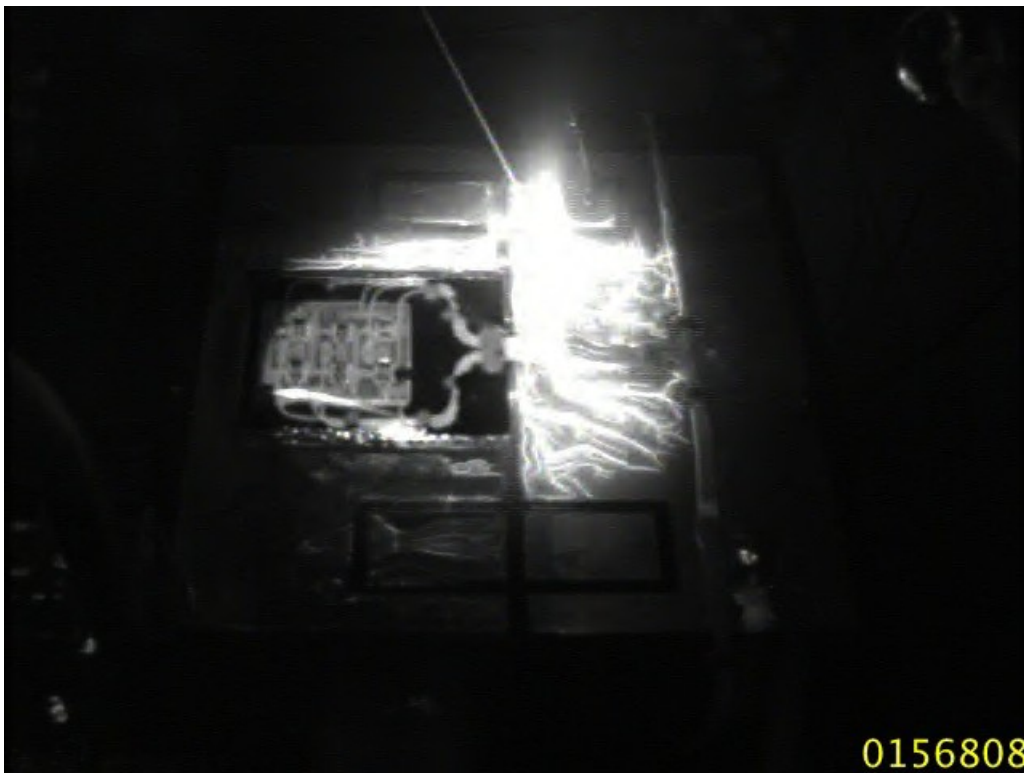Figure 30: Photograph of the mitigation coupon

Figure 31: Video image of surface flashover on the mitigation coupon. Note that the diode board is protected from the surface flashover.

Table 6: Thresholds of arc inception for different coupon designs. The number for the South Pole denotes the potential of the conductive part to the surrounding plasma. The number of the North Pole denotes typical surface potential of Ag-TF thermal insulator.

	Baseline coupon	Mitigation coupon
South Pole	-80 ~ -90V at CFRP	-340 ~ -360V at harness/adhesive border
North Pole (small arc)	-1500V at Ag-TF edge	-7400 ~ -8300V at harness/adhesive border
North Pole (surface flashover)	-7000V	-8500 ~ -9500V

Figure 33: Coupon used for the extreme test. Photograph taken before the test. Damages on Ag-TF film are due to previous tests.
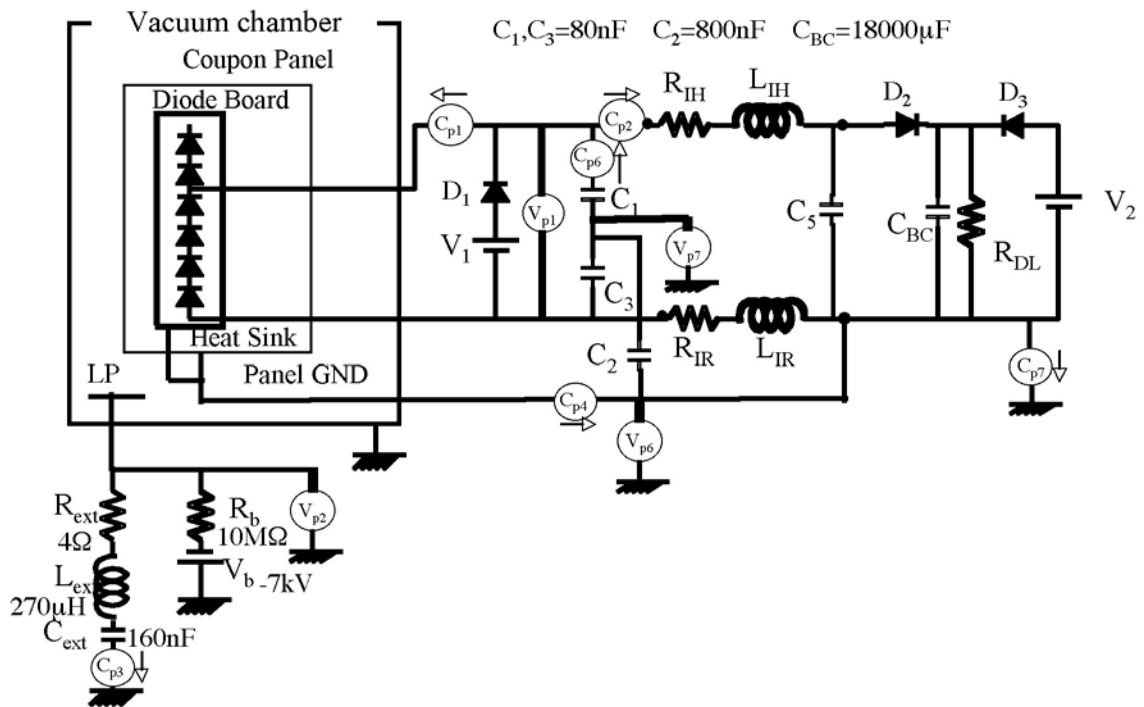
Figure 34: Circuit layout used for the extreme test

Table 7: Summary of extreme test results

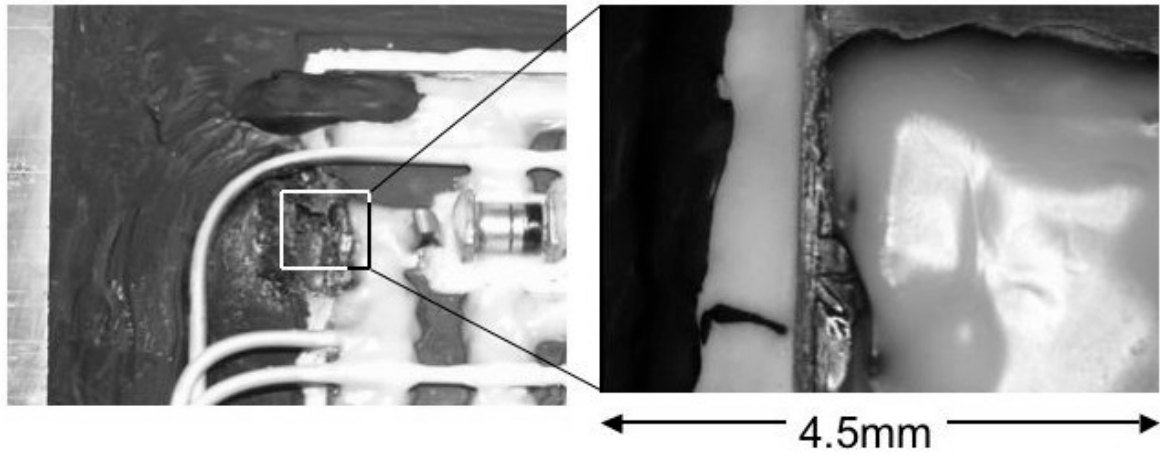| String voltage, V	String current, A	Total number of primary arc	Total number of temporary sustained arc	Total number of permanent sustained arc	Maximum duration of temporary sustained arc, μs	Experiment time (m:s)
40	2.7	182	0	0	NA	1:00
80	2.7	222	0	0	NA	1:50
110	2.7	1006	4	0	60	6:34
110	4	1007	3	0	50	9:17
150	2.7	92	1	1	>180	0:30

Figure 35: Photograph of sustained arc location after the extreme test (left) and close-up photograph inside the square at center taken before the extreme test (right).